

Subduction initiation and back-arc opening north of Neo-Tethys: Evidence from the Late Cretaceous Torbat-e-Heydarieh ophiolite of NE Iran

Hadi Shafaii Moghadam^{1,2,†}, R.J. Stern³, W.L. Griffin², M.Z. Khedr⁴, M. Kirchenbaur^{5,6}, C.J. Ottley⁷, S.A. Whattam⁸, J.-I. Kimura⁹, G. Ghorbani¹, S. Gain², S.Y. O'Reilly², and A. Tamura¹⁰

¹School of Earth Sciences, Damghan University, Damghan 36716-41167, Iran

²ARC Centre of Excellence for Core to Crust Fluid Systems and GEMOC ARC National Key Centre, Department of Earth and Planetary Sciences, Macquarie University, NSW 2109, Australia

³Geosciences Department, University of Texas at Dallas, Richardson, Texas 75083-0688, USA

⁴Department of Geology, Faculty of Science, Kafrelsheikh University, 33516 Kafr Elsheikh, Egypt

⁵Institut für Mineralogie, Leibniz Universität Hannover, Germany

⁶Universität zu Köln, 50674 Köln, Germany & Steinmann-Institut, Universität Bonn, Germany

⁷Department of Earth Sciences, Northern Centre for Isotopic and Elemental Tracing, University of Durham, Durham, DH1 3LE, UK

⁸Department of Geosciences, King Fahd University of Petroleum and Minerals, Dhahran 31261, Saudi Arabia

⁹Department of Solid Earth Geochemistry, Japan Agency for Marine-Earth Science and Technology (JAMSTEC), Natsushima-Cho 2-15, Yokosuka 237-0061, Japan

¹⁰Department of Earth Sciences, Kanazawa University, Ishikawa 920-1192, Japan

ABSTRACT

How new subduction zones form is an ongoing scientific question with key implications for our understanding of how this process influences the behavior of the overriding plate. Here we focus on the effects of a Late Cretaceous subduction-initiation (SI) event in Iran and show how SI caused enough extension to open a back-arc basin in NE Iran. The Late Cretaceous Torbat-e-Heydarieh ophiolite (THO) is well exposed as part of the Sabzevar-Torbat-e-Heydarieh ophiolite belt. It is dominated by mantle peridotite, with a thin crustal sequence. The THO mantle sequence consists of harzburgite, clinopyroxene-harzburgite, plagioclase lherzolite, impregnated lherzolite, and dunite. Spinels in THO mantle peridotites show variable Cr# (10–63), similar to both abyssal and fore-arc peridotites. The igneous rocks (gabbros and dikes intruding mantle peridotite, pillowed and massive lavas, amphibole gabbros, plagiogranites and associated diorites, and diabase dikes) display rare earth element patterns similar to MORB, arc tholeiite and back-arc basin basalt. Zircons from six samples, including plagiogranites and dikes within mantle peridotite, yield U-Pb ages of ca. 99–92 Ma,

indicating that the THO formed during the Late Cretaceous and was magmatically active for ~7 m.y. THO igneous rocks have variable $\epsilon\text{Nd}(t)$ of +5.7 to +8.2 and $\epsilon\text{Hf}(t)$ ranging from +14.9 to +21.5; zircons have $\epsilon\text{Hf}(t)$ of +8.1 to +18.5. These isotopic compositions indicate that the THO rocks were derived from an isotopically depleted mantle source similar to that of the Indian Ocean, which was slightly affected by the recycling of subducted sediments. We conclude that the THO and other Sabzevar-Torbat-e-Heydarieh ophiolites formed in a back-arc basin well to the north of the Late Cretaceous fore-arc, now represented by the Zagros ophiolites, testifying that a broad region of Iran was affected by upper-plate extension accompanying Late Cretaceous subduction initiation.

INTRODUCTION

Ophiolites are fragments of upper mantle and oceanic crust (Coleman, 1977; Nicolas, 1989) and are often tectonically incorporated into continental margins during continent-continent and arc-continent collisions (Dilek and Flower, 2003), ridge-trench interactions (Lagabriele et al., 2000), and/or subduction-accretion events (Cawood, 1989). Ophiolites and their dismembered equivalents are especially common in suture zones in both collisional and accretionary orogens of Neoproterozoic and Phanerozoic age (e.g., Furnes et al., 2014; Hébert et al., 2012; Saccani et al., 2013). Dilek and Furnes (2011)

classified ophiolites into continental margin, mid-ocean-ridge, plume, supra-subduction zone, volcanic arc, and accretionary types, according to their tectonic settings. Evidence is growing that many ophiolites form during subduction initiation in a fore-arc setting (Whattam and Stern, 2011), and this concept is useful for understanding the Late Cretaceous ophiolites of the Zagros Mountains in Iran (Moghadam and Stern, 2011; Moghadam et al., 2010).

The emplacement of an ophiolite on continental crust can occur via various mechanisms, including obduction, subduction and then exhumation of oceanic lithosphere, or even through trapping and compression of oceanic basins between two neighboring continental blocks, as is the case for NE Iran ophiolites. Despite the fact that it is geodynamically difficult to emplace ophiolites that form anywhere other than the fore-arc (Stern, 2002), ophiolites are known to form in other extensional settings such as marginal basins or back-arc basins. Back-arc basins need strong extension to open, and this can be achieved as a result of subduction initiation (SI). Back-arc extension is not as easily accomplished if regional compression causes induced SI, but is expected to accompany spontaneous SI, due to the large lateral density contrasts across the lithospheric weakness separating the pertinent plates (Stern, 2004; Stern and Gerya, 2017). Spontaneous SI (i.e., when oceanic lithosphere begins to sink vertically before down-dip motion is established), will cause extension in the overlying plate, and this can open a back-arc

[†]Present address: FB4–Dynamics of the Ocean Floor, GEOMAR, Helmholtz-Zentrum für Ozeanforschung Kiel, Wischhofstr. 1-3, 24148 Kiel, Germany; hshafaei@geomar.de.

basin. How subduction initiation causes extension in the overlying plate also depends on plate configuration and relative motions, thickness of the subducting oceanic slab, and whether SI is spontaneous or induced.

Marginal basin is a general term for basins of unknown origin associated with continental margins and island arcs. Back-arc basins are a type of marginal basin that open at a convergent plate margin behind an active magmatic arc. Most back-arc basins are associated with oceanic arcs, although rifting of continental lithosphere also produces back-arc basins (i.e., ensialic back-arc basins) (Gerya, 2011; Stern, 2002). Back-arc ophiolites are represented by mid-ocean-ridge basalt (MORB)-like, back-arc basin basalt (BABB)-like, and calc-alkaline-type intrusions and lavas, generated by partial melting of a MORB-type mantle source (through mantle wedge flow; e.g., Long and Wirth, 2013) into the sub-arc mantle wedge (Saccani et al., 2008). In many cases, the tectonic setting of ophiolites is obscured by alteration and deformation, so that workers rely heavily on relict mineralogy and immobile trace-element geochemistry to resolve the original tectonic setting. This approach is problematic because back-arc basins and fore-arc ophiolites share many geochemical and petrographic features and can be difficult to distinguish solely on a basis of petrology and

geochemistry; other considerations are required to distinguish back-arc and fore-arc ophiolites. This report addresses this problem by focusing on a well-preserved ophiolite belt in NE Iran that clearly formed in a back-arc, subduction-initiation (SI) setting. Our research supports results from recent International Ocean Discovery Program (IODP) drilling in the Philippine Sea indicating that extensional magmatism related to subduction initiation can affect much larger regions than just the immediate fore-arc environment (Hickey-Vargas et al., 2018).

The Sabzevar-Torbat-e-Heydarieh ophiolites (STHO) are excellent examples of Late Cretaceous ophiolites of Iran. The STHO are exposed over a large area of NE Iran, $\sim 130 \times 400$ km (Fig. 1). From a regional-tectonic perspective, the STHO are situated in a back-arc setting, separated by ~ 600 km from the Zagros fore-arc ophiolites (Moghadam and Stern, 2011; Monsef et al., 2018), the Urumieh-Dokhtar Magmatic Belt (UDMB) and continental crust of the Lut block (Fig. 2). The faulted contact between the southernmost STHO and Ediacaran-Cambrian (Cadomian) basement to the south is exposed on the southern margin of the STHO (Fig. 3). Cadomian basement comprises granitoids, gabbros, rhyolites, and pyroclastic rocks with ages of 531–553 Ma (Moghadam et al., 2017b). The

STHO were exhumed during latest Cretaceous–Paleogene extension associated with formation of the Oryan Basin (Fig. 3). This is also confirmed by low-temperature thermo-chronometric and structural evidence, which show that uplift of the ophiolite domain was accompanied by dextral transpression beginning in the early Paleocene (ca. 60 Ma) and ending in the Miocene-Pliocene (5 Ma) (Tadayon et al., 2018). This conclusion is supported by the presence of an early Paleocene unconformity and deposition of middle Paleocene conglomerates which seal the STHO ophiolites. These conglomerates were produced by the erosion of the exhuming ophiolites during dextral transpression (Tadayon et al., 2018).

The modern episode of subduction within the Zagros oceanic realm (Neotethys Ocean) began at 104–98 Ma, as determined by zircon U-Pb dating of Zagros fore-arc ophiolites (Moghadam et al., 2013; Moghadam and Stern, 2015). Late Cretaceous subduction initiation was accompanied by a major change in the direction and velocity of Arabia-Eurasia convergence (Agard et al., 2007). We suggest that Late Cretaceous spontaneous SI caused the observed change in plate motion; that subsidence of Mesozoic Neotethys lithosphere commenced along a transform margin adjacent to buoyant Eurasian lithosphere, causing proto-fore-arc seafloor spreading and producing the Zagros ophiolites (Moghadam and Stern, 2011; Moghadam et al., 2010). Foundering Neotethys oceanic lithosphere induced extension on the southern margin of Eurasia, producing back-arc basins, tilting of crustal blocks, uplift and intense erosion of the Iranian plateau, as well as core complex exhumation in some parts of the Iranian plateau (Malekpour-Alamdari et al., 2017; Moritz et al., 2006; Verdel et al., 2007). For testing the Late Cretaceous SI model for southern Eurasia, it is essential to understand the significance of the Late Cretaceous back-arc basins in NE Iran, of which the Sabzevar-Oryan-Cheshmehshir-Torbat-e-Heydarieh ophiolite is the largest representative (Fig. 3). Besides the suspected back-arc basins in NE Iran, there are several other Late Cretaceous oceanic basins (ophiolites) whose opening seems to be related to the Late Cretaceous extension within the Iranian plateau caused by SI along the Zagros suture zone. These ophiolites include the Khoy ophiolite in NW Iran (e.g., Khalatbari-Jafari et al., 2004) and scattered ophiolitic slices along the Talysh-Qare Dagh Mountains in NNW Iran (e.g., Burtman, 1994; Omidvar et al., 2018).

We present here the results of our study of Late Cretaceous mantle peridotites, gabbros, lavas, and plagiogranites from the Torbat-e-Heydarieh ophiolite. We provide zircon U-Pb ages for six samples of geochemically distinct plagiogranites,

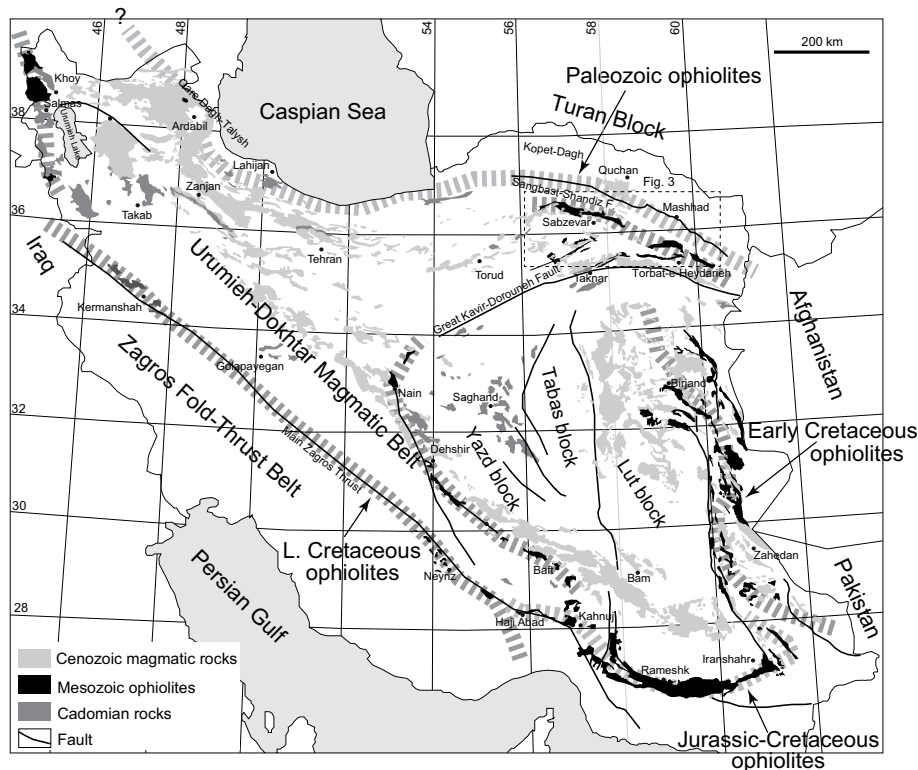


Figure 1. Simplified geological map of Iran emphasizing Cadomian rocks, the main ophiolitic belts (thick dashed lines) and Cenozoic magmatic rocks.

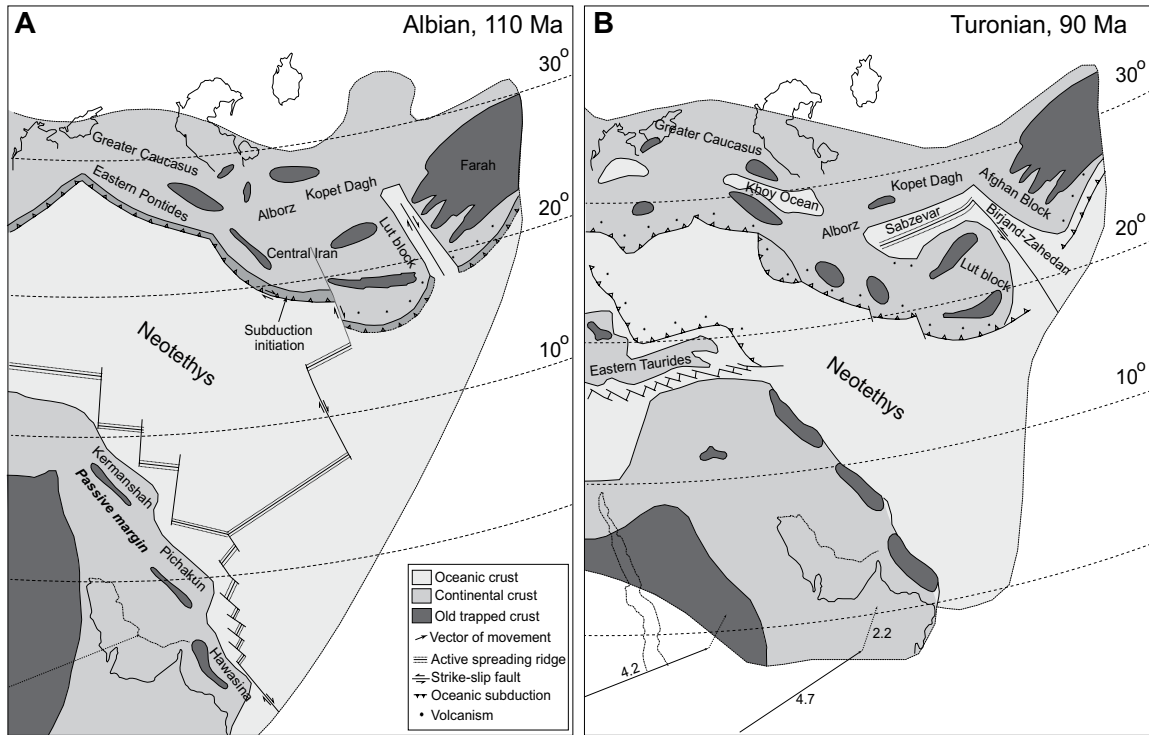


Figure 2. (A) and (B) Schematic model showing the opening and evolution of the Sabzevar-Torbat-e-Heydariieh back-arc basin relative to the Zagros, Neotethyan Ocean (modified after Dercourt et al., 1986; Kazmin et al., 1986).

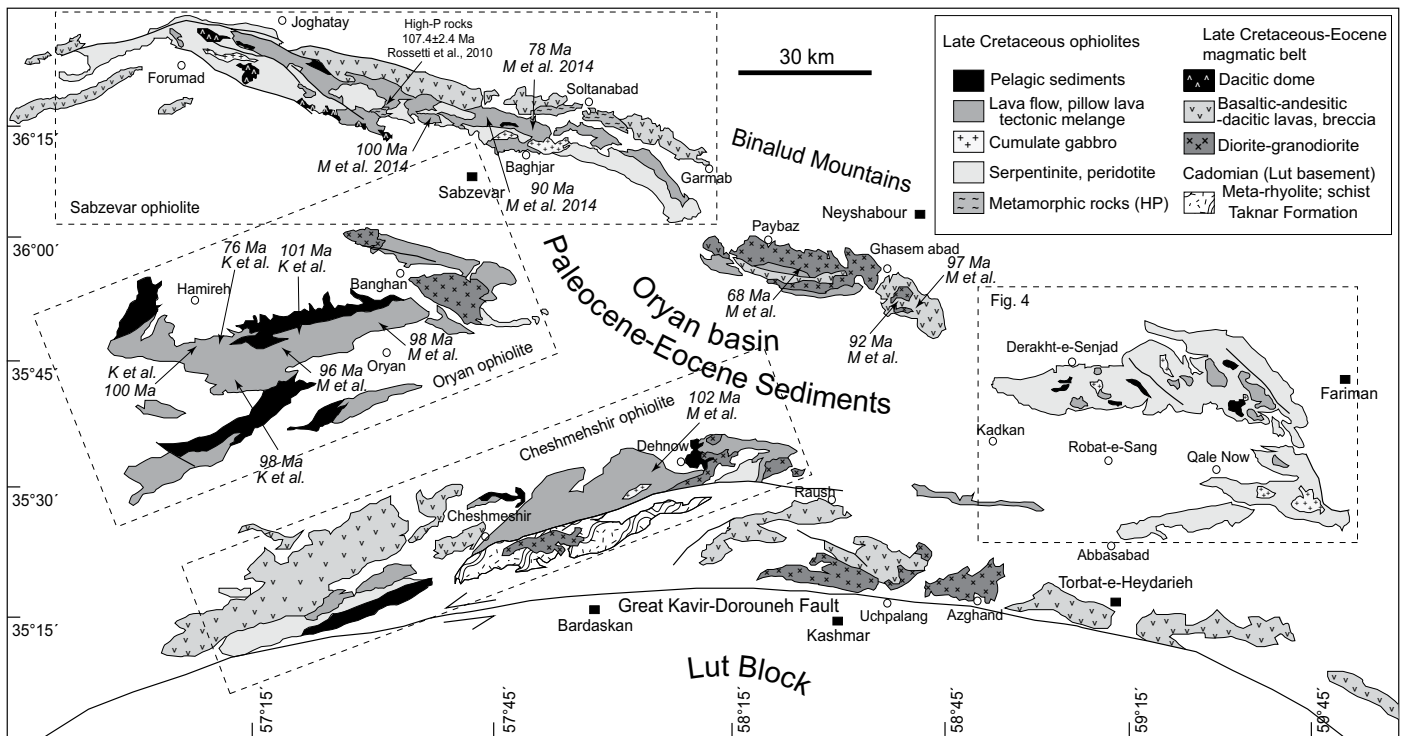


Figure 3. Geological map of the Sabzevar-Torbat-e-Heydariieh region, north of the Dorouneh Fault, with emphasis on the distribution of ophiolitic and arc-related rocks. (M et al.—Kazemi et al., 2019; K et al.—Kazemi et al., 2019; M et al., 2014—Moghadam et al., 2014a).

gabbros, and dikes and compare these with geochronological data from the Sabzevar ophiolite to the NW (Fig. 3). Peridotite mineral compositions as well as major, trace-, and rare-earth element data and bulk rock Nd-Hf and zircon Hf isotopes for selected samples are used to constrain the tectonic setting of the different magmatic suites. We show that the mantle rocks and magmatic rocks were generated during back-arc basin extension and use these results and their magmatic-stratigraphic associations to suggest that magmatism occurred in response to SW-directed rollback of a NE-dipping subduction zone during SI (Fig. 2).

GEOLOGICAL SETTING

The STHO is bordered to the north by the major Sangbast-Shandiz strike-slip fault delimiting the Binalud Mountains (Fig. 1). To the south, the STHO is bounded by the major Great Kavir-Dorouneh sinistral strike-slip fault (Figs. 1 and 3). The STHO comprises four main regions where ophiolites crop out (Fig. 3), separated by

the Paleocene-Eocene Oryan sedimentary basin: (1) NNW of Sabzevar (the Sabzevar ophiolite, studied by Moghadam et al., 2014b, 2015; Nasrabad et al., 2011; Omrani et al., 2013; Rossetti et al., 2010, 2014; Shojaat et al., 2003); (2) SSW of Sabzevar (Oryan ophiolite, no published data); (3) Cheshmehshir in the far south (Maghfouri et al., 2016); and (4) north of Torbat-e-Heydarieh, the focus of this study.

The STHO lies between the Lut block in the south and the Kopeh-Dagh (Turan platform; Thomas et al., 1999) in the north. The STHO formed during the Late Cretaceous (Moghadam and Stern, 2015) and contains a well-preserved mantle sequence, but some parts are fragmented and sheared. There is consensus that the STHO formed above a supra-subduction zone (SSZ) setting, as most Sabzevar ophiolite lavas show appropriate geochemical signatures (Ghazi et al., 1997; Moghadam et al., 2014a; Shojaat et al., 2003). Sabzevar mantle peridotites have spinels with both MORB-like ($Cr\# < 50\%$) and SSZ-type ($Cr\# > 50\%$) signatures but most peridotite spinels

have high $Cr\# (> 50)$ with low TiO_2 and resemble those of SSZ peridotites (Moghadam et al., 2014a). Some Sabzevar ophiolite pillow lavas have ocean-island basalt (OIB)-like whole-rock compositions, suggesting a plume or subcontinental lithospheric mantle source. The Sabzevar ophiolite is covered by Late Campanian to Early Maastrichtian (ca. 75–68 Ma) pelagic sediments. Sabzevar plagiogranites yield zircon U-Pb ages of 99.9–77.8 Ma (Moghadam et al., 2014a). Magmatic rocks of the Sabzevar ophiolite have positive $\epsilon Nd(t)$ values (+5.4 to +8.3) and most have high $^{207}Pb/^{204}Pb$, indicating a significant contribution of subducted sediments to their mantle source (Moghadam et al., 2014a).

The Torbat-e-Heydarieh ophiolite (THO) constitutes the southeasternmost of the four STHO outcrops, covering an area 60 km long and 50 km wide (Fig. 4). The THO shows no contact with older rocks and is unconformably overlain by Paleocene-Eocene conglomerates and sandstones. The THO is mostly composed of mantle peridotites including lherzolites, impregnated

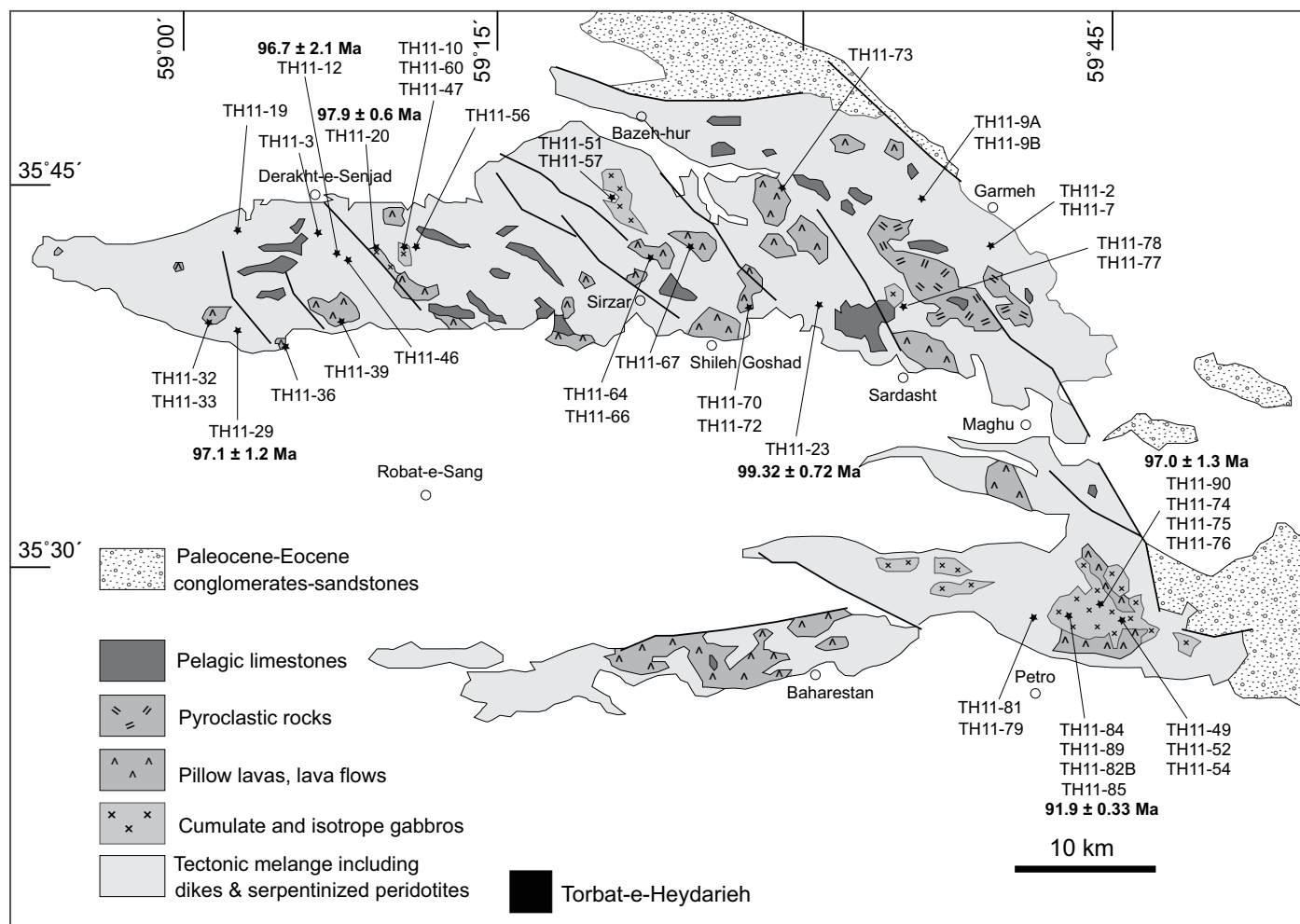


Figure 4. Simplified geological map of the Torbat-e-Heydarieh ophiolite (modified after Vaezi Pour et al., 1992).

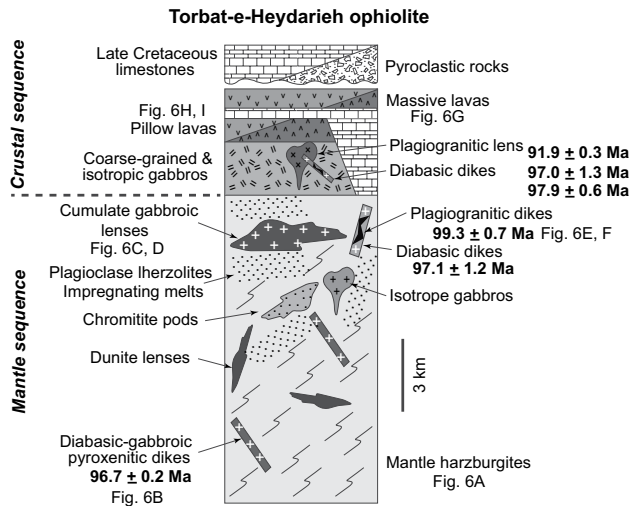


Figure 5. Simplified stratigraphic column displaying idealized internal lithologic successions in the Torbat-e-Heydarieh ophiolite.

lherzolites, minor harzburgites, and discordant dunites and chromitite lenses (Figs. 5, 6A). Harzburgites with 2–3 modal% clinopyroxene and plagioclase-lherzolites are also common. Dunites also occur as small veins and pods/lenses within the harzburgite. Diabasic-gabbroic-pyroxenitic dikes crosscut the mantle sequence and in most cases are boudinaged (Fig. 5). Diabasic-gabbroic dikes are locally converted into rodingite (Fig. 6B). Some diabasic dikes are metamorphosed to greenschist or lower amphibolite facies. Small intrusions of cumulate and fine-grained isotropic gabbro and pyroxenite (Figs. 6C, 6D) are common in harzburgites and lherzolites; pyroxene-rich gabbroic dikes are also common within these gabbros. Cumulate gabbroic lenses occasionally are layered, characterized by plagioclase-rich (anorthosite) and orthopyroxene

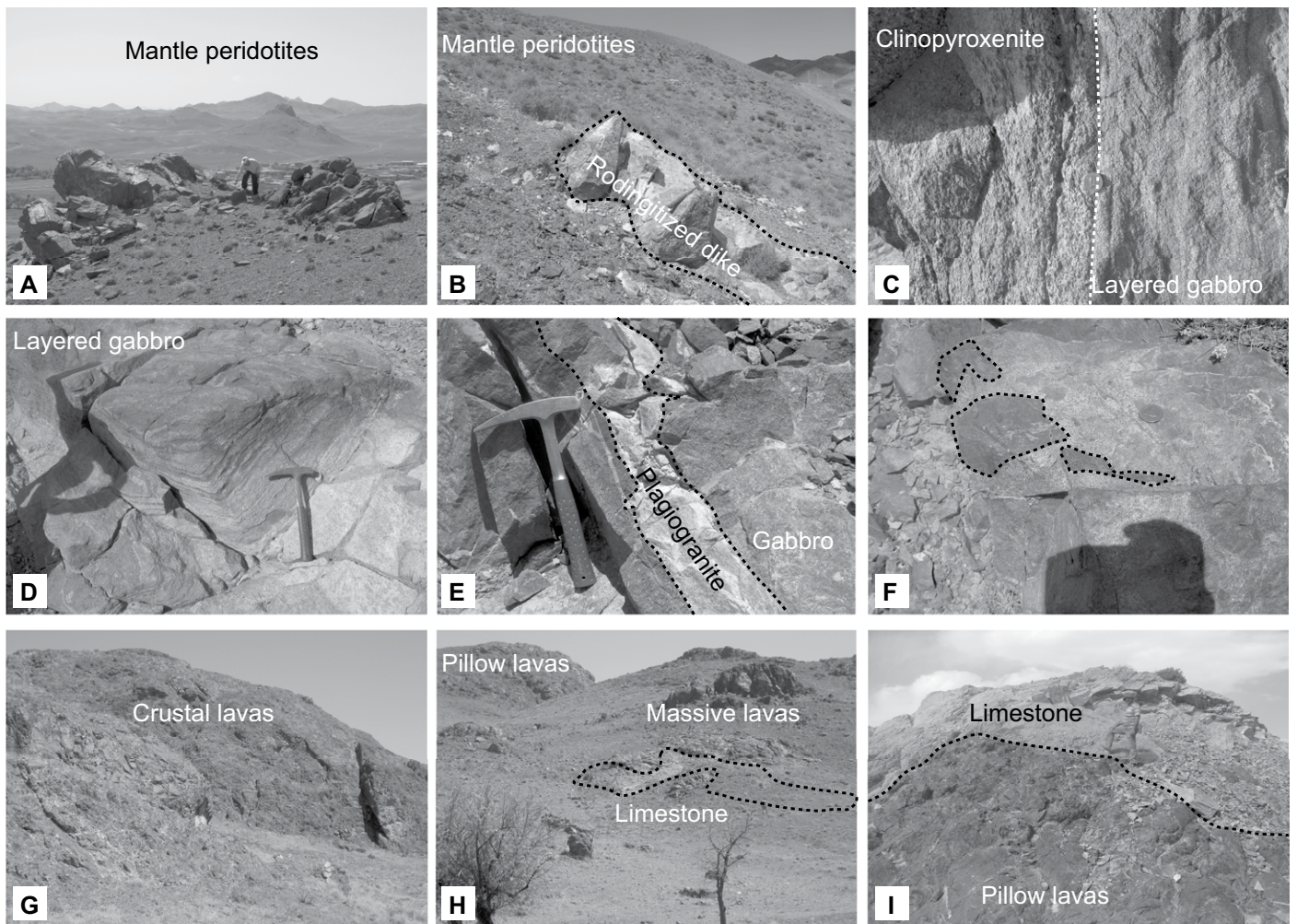


Figure 6. Outcrop photos of the Torbat-e-Heydarieh ophiolite (THO) rock units. (A) Outcrops of mantle peridotites. (B) Rodingitized dikes within the THO mantle peridotites. (C) Outcrop of interlayered cumulate gabbros (layered gabbros) and clinopyroxenites. (D) Small intrusions of cumulate (layered) gabbros within the THO mantle sequence. (E) Plagiogranitic dikes within the mantle gabbroic intrusions. (F) Angular gabbroic xenoliths within the plagiogranitic pockets. (G) Outcrops of crustal massive and pillow lavas. (H, I) Late Cretaceous (Cenomanian to Turonian, ca. 99–90 Ma) pelagic sediments are interlayered with and conformably cover the lavas.

(Opx)- and clinopyroxene (Cpx)-rich (olivine-bearing) bands (olivine-bearing melanocratic gabbros) (Fig. 6D). The gabbroic sequence is crosscut by diabasic and microgabbroic to more-evolved plagiogranitic dikes or small pockets (Fig. 6E). Some dikes within the gabbros also intrude the underlying peridotites. In some cases, angular gabbroic xenoliths are found within the plagiogranitic pockets (agmatite, Fig. 6F). Late plagiogranitic dikes were injected into both gabbros and underlying peridotites.

The THO crustal sequence is more poorly exposed than the mantle section but includes massive and pillow lavas (Fig. 6G), isotropic and coarse-grained massive gabbros, and plagiogranite lenses/dikes within the gabbros (Fig. 5). The contact between the mantle sequence and crustal rocks in most cases is tectonized, but in some cases, the mantle rocks are overlain by cumulate gabbros or by crustal lavas and pelagic limestones. The presence of pelagic limestone on top of the mantle section suggests that Late

Cretaceous extension on the seafloor was locally amagmatic. Crustal gabbros differ from mantle gabbros by containing more diabasic dikes and large plagiogranitic lenses, but plagiogranitic dikes are also common. Lava flows are slightly metamorphosed to greenschist or lower amphibolite facies. Other rocks from both crustal and mantle sequences show no trace of metamorphism, but instead they show slight to moderate alteration. High-temperature alteration of mantle dikes into rodingite is also common. Pillow lavas show pyrite-chalcocopyrite mineralization. Massive and pillow lavas are occasionally tectonically interlayered with peridotites. There is no obvious geochemical difference between most pillow and massive lavas (see next section). Late Cretaceous (Cenomanian to Turonian, ca. 99–90 Ma) pelagic sediments and pyroclastic rocks are interlayered with and conformably cover the lavas (Figs. 6H, 6I). Cold breccia, including basaltic fragments set in a pelagic limestone matrix, is abundant. THO mélanges

include serpentinites, lavas, and pelagic sediments. These mélanges are especially abundant in the Sabzevar ophiolites, where various ophiolitic units, Paleocene-Eocene magmatic rocks, and shallow-water limestones are dispersed with serpentinites, showing that these mélanges are related to Eocene or younger deformation (Moghadam et al., 2014a).

PETROGRAPHY

Lherzolites are the predominant THO mantle rocks; they contain serpentinized olivine, orthopyroxene, and large clinopyroxenes (Fig. 7A). Nearly all lherzolite samples are moderately (20%–30%) serpentinized. Vermicular brown spinel is abundant and generally intergrown with clinopyroxene. Harzburgites are minor and contain serpentinized olivine and orthopyroxene porphyroclasts with fine-grained clinopyroxene (2%–3%, Fig. 7C) and deep brown spinel. Serpentinization of harzburgites

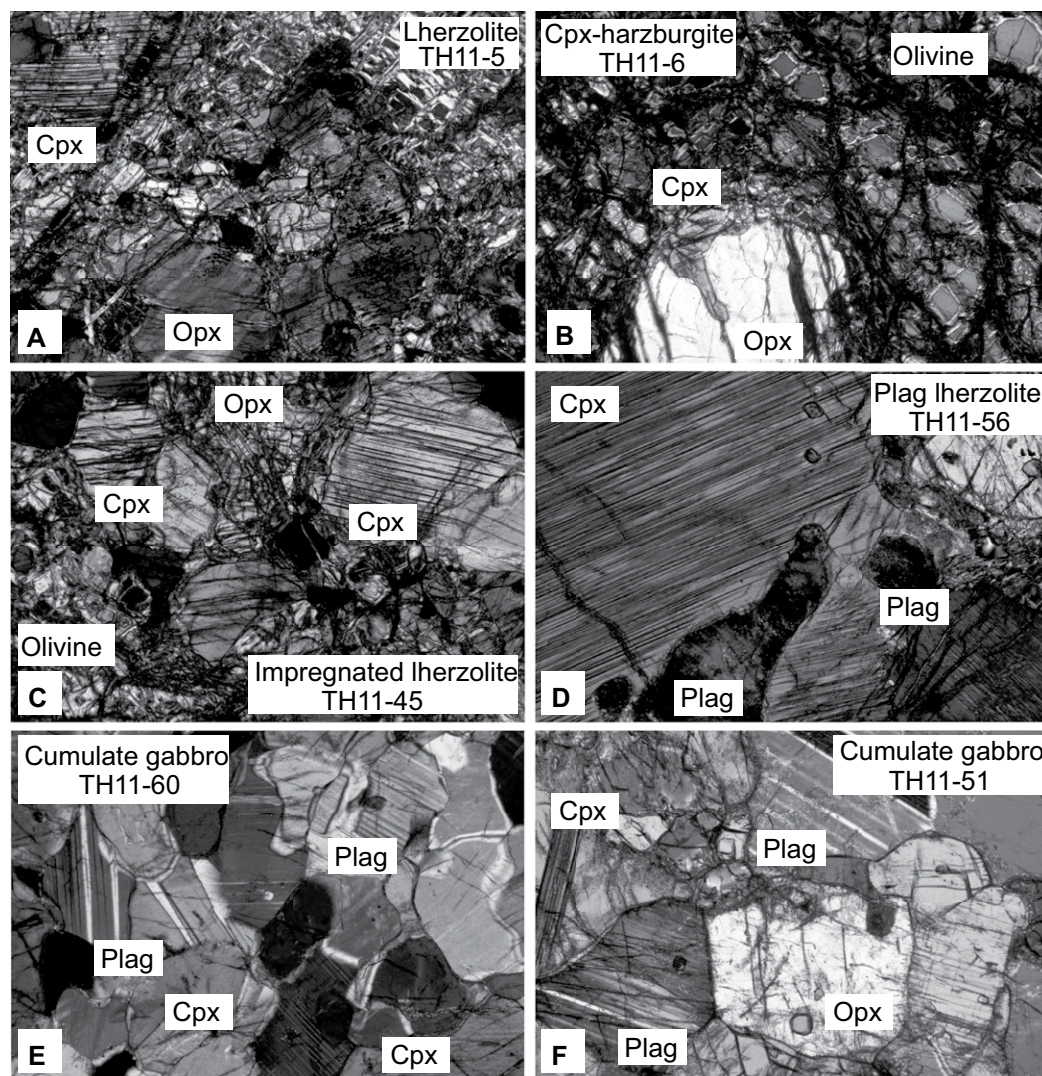


Figure 7. Photomicrographs of the Torbat-e-Heydariieh ophiolite (THO) mantle peridotites and gabbros. (A) Orthopyroxene (Opx), clinopyroxene (Cpx), and serpentinized olivine in lherzolites. (B) Serpentinized olivines, Opx, and Cpx grains as embayment within the Opx in Cpx-harzburgites. (C) Serpentinized olivine, Opx, and Cpx aggregates within the impregnated lherzolites. (D) Coarse-grained Cpx crystals and altered plagioclase (Plag) in plagioclase-bearing lherzolites. (E) and (F) Opx, Cpx, and plagioclase in mantle cumulate gabbros.

(50%–60%) is greater than in lherzolites (20%–30%). The content of clinopyroxene is higher in Cpx-harzburgites (3%–5%). Here, fine clinopyroxenes occur in embayments of orthopyroxene porphyroclasts (Fig. 7B), associated with vermicular spinels (Fig. 8A). Part of the THO mantle section was impregnated with a percolating basaltic melt which filtered through peridotites, crystallizing plagioclase and clinopyroxene. Impregnated lherzolites have more coarse-grained clinopyroxene aggregates and lighter-brown spinel compared to normal lherzolites (Fig. 7C). Plagioclase lherzolites show traces of altered plagioclase (5–7 modal%) along with melt-impregnated clinopyroxenes (up to 20%–30%) and light brown vermicular spinel.

Large clinopyroxenes enclose plagioclase and brown spinels (Figs. 6D and 7B). Plagioclase also occurs at the contact of orthopyroxene with impregnated clinopyroxenes (Fig. 8C). Blebs of sulfide minerals are also observed. Clinopyroxene accumulation in plagioclase lherzolites makes these rocks similar to olivine websterites (Fig. 9A). Plagioclase lherzolites show melt-assisted crystallization of new olivine grains in plagioclase and clinopyroxene embayments (Fig. 8C). Dunites are altered (50%–70% serpentinization) with mesh-textured olivines (>90%) and coarse-grained black spinel. Spinel contains abundant inclusions of serpentinized olivine, clinopyroxene, and amphibole (Fig. 8D). Amphibole inclusions are altered to chlorite.

Gabbroic lenses within peridotites vary from gabbro (~1%–2% Opx) to gabbronorite (10%–30% Opx; Fig. 9B). Cumulate gabbros are heterogeneous, with dark bands rich in clinopyroxene, orthopyroxene and minor plagioclase, and whitish bands rich in plagioclase with minor clinopyroxene. Olivine is rare, whereas coarse-grained, subhedral orthopyroxene and anhedral clinopyroxene are the main components of cumulate gabbros (Figs. 7E, 7F). Plagioclase is interstitial between pyroxene crystals (Figs. 8E, 8F). Fine-grained, isotropic gabbros containing plagioclase, orthopyroxene, and clinopyroxene are also common in the mantle sequence, closely associated with cumulate gabbros. Occasional primary brown amphiboles also occur as interstitial laths between other minerals. Rodingitized dikes contain fine-grained hydrogrossular, rare diopside, and wollastonite as well as pectolite.

Coarse-grained crustal plutonic rocks contain plagioclase and amphibole in diorites and clinopyroxene and plagioclase in gabbros. Some gabbros contain interstitial amphibole. Plagiogranites have granular texture and are dominated by plagioclase, quartz, and amphibole with secondary epidote, chlorite, sericite, iron oxide, and titanite. Apatite and zircon are minor components. Plagiogranites can be petrographically divided into tonalites and diorites with more amphibole. Granophyric intergrowths of plagioclase and quartz are also common in these rocks.

Diabasic dikes are fine-grained and contain magnesio-hornblende and sodic plagioclase. Pillow lavas contain clinopyroxene microphenocrysts, plagioclase microlites, and palagonitized glass. Fine-grained clinopyroxene is also common in the groundmass. Calcite, chalcedony, titanite, sericite, epidote, prehnite, and chlorite are secondary phases.

Pillow lavas display hyaloporphyritic to intersertal texture with clinopyroxene and plagioclase micro-phenocrysts. Massive lavas are similar to pillow lavas but are less altered. The glassy groundmass of some massive lavas is altered into chlorite and clay, but most are holocrystalline without glass.

ANALYTICAL METHODS

We used six main analytical procedures to study THO rocks: (1) JEOL wavelength dispersive electron probe X-ray micro-analyzer (JXA 8800R) to determine the composition of minerals; (2) inductively coupled plasma–atomic emission (ICP-AES) and inductively coupled plasma–mass spectrometry (ICP-MS) to determine whole-rock contents of major- and trace elements; (3) cathodoluminescence (CL) imaging of zircons; (4) sensitive high-resolution ion microprobe (SHRIMP) analyses to determine zircon U–Pb

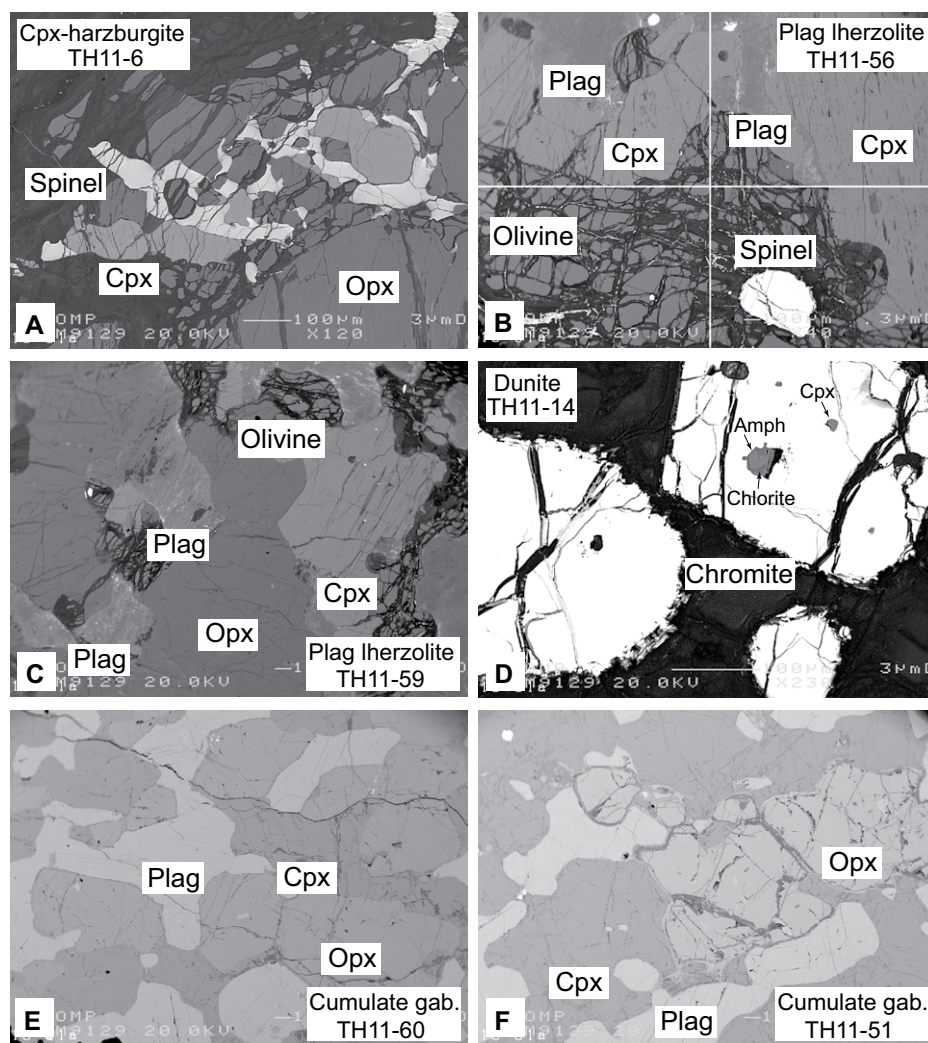


Figure 8. Back-scattered images of Torbat-e-Heydarieh ophiolite (THO) mantle rocks. (A) Association of clinopyroxene (Cpx) and vermicular spinels at the embayments of orthopyroxene (Opx) porphyroclasts in Cpx-harzburgites. (B) Altered plagioclase (Plag) enclosed by large Cpx grains in plagioclase lherzolites. (C) Olivine, Opx, Cpx, and plagioclase in plagioclase lherzolites. (D) Cpx and chloritized amphibole (Amph) inclusions in the chromite of dunites. (E, F) Cumulate texture in mantle cumulate gabbros (gab) with early crystallized Opx and Cpx and late-stage, interstitial plagioclase crystals.

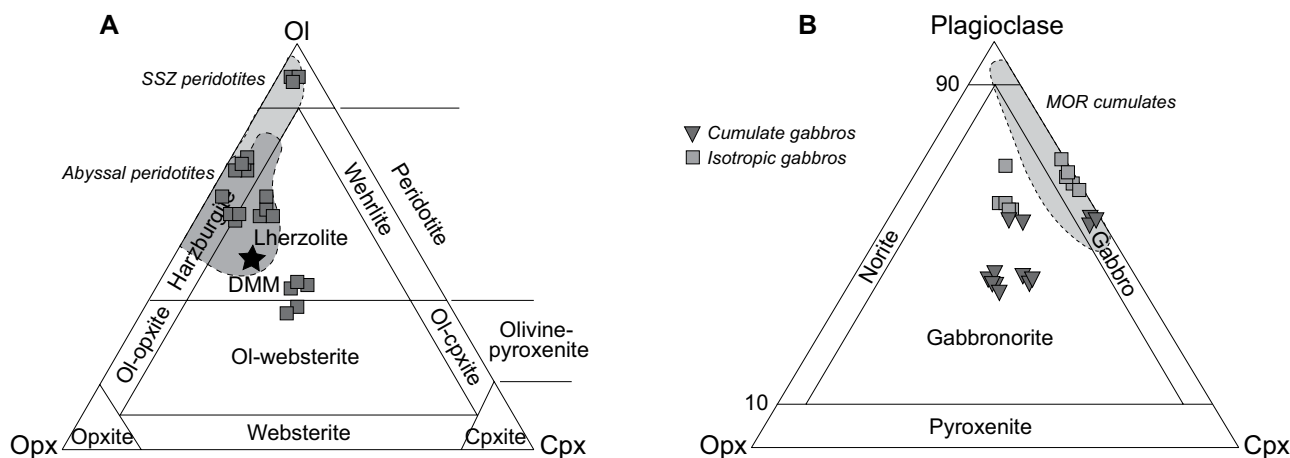


Figure 9. Modal composition of Torbat-e-Heydarieh ophiolite mantle peridotites (A) and gabbros (B). MOR—mid-ocean ridge; SSZ—supra-subduction zone; DMM—depleted MORB mantle; Cpx—clinopyroxene; Ol—olivine; Opx—orthopyroxene.

ages; (5) laser ablation–inductively coupled plasma mass spectrometry (LA-ICPMS) analyses to determine zircon U–Pb ages and to analyze the trace-element compositions of clinopyroxene and orthopyroxene from mantle peridotites and gabbros; and (6) multi collector–inductively coupled plasma–mass spectrometry (MC-ICP-MS) equipped with LA for in situ analysis of zircon Hf isotopic compositions. The same MC-ICP-MS was used to analyze the isotopic compositions of Nd and Hf in whole-rock samples.

We studied ~100 samples for petrography, 13 polished thin sections for electron microprobe analysis, 39 for whole-rock major- and trace-element compositions, six for U–Pb zircon ages, eight for whole-rock Nd and Hf analyses, six for in situ mineral trace elements, and six for in situ Lu–Hf isotope analyses of zircons. The Nd and Hf isotopic compositions discussed below are corrected for 100 Ma of radiogenic ingrowth. The details of each technique are given in Electronic Appendix A¹.

WHOLE-ROCK GEOCHEMISTRY

Three mantle peridotites, 14 mantle gabbros, 10 pillowed and massive lavas, four amphibole gabbros, two mantle-intruding dikes, and six plagiogranites and associated diorites and diabase dikes samples were selected for whole-rock analysis. Sample locations are shown on Figure 4. The analyzed samples are characterized by variable loss on ignition; 0.6–4.2 wt% for crustal rocks, 5.9–11.7 wt% for peridotites and 0.6–5.8 wt% for mantle gabbros. Because of the mobility of

some major and trace elements during alteration, emphasis is placed on immobile trace elements such as the rare earth element (REE) and high field strength elements (HFSE) to evaluate the original composition and tectono-magmatic setting of Torbat-e-Heydarieh magmatic rocks. Fluid-mobile elements such as Cs, Rb, U, Pb, and Sr may be discussed but are generally deemphasized in the following sections. Similarly, to avoid the effects of alteration and seawater exchange on isotopic composition of the rocks, alteration-resistant Nd and Hf isotopes are reported.

Mantle Units

Harzburgite has low contents of CaO and Al₂O₃ (~1.6 wt%), whereas Cpx-harzburgite and plagioclase lherzolite contain more CaO (~2.3 and ~8.9 wt%, respectively) and Al₂O₃ (~2.3 and ~5.1 wt%, respectively) (Supplementary Table DR1; see footnote 1). Harzburgites show highly depleted REE patterns, with steep slopes from LREEs (light REEs) to MREEs (middle REEs) (Fig. 10A). REE abundances are higher in Cpx-harzburgite and plagioclase lherzolite with nearly flat patterns from MREEs to HREEs, but with steep slope from LREEs to MREEs. These patterns are similar to those of the cumulate gabbros (Fig. 10A). Enrichment in MREEs to HREEs (heavy REEs) for Cpx-harzburgite and plagioclase lherzolite is consistent with the formation of clinopyroxene by metasomatism. Enrichment in fluid-mobile elements such as U, Rb, Ba, Sr, and Pb relative to LREEs is characteristic of THO mantle peridotites.

Mantle gabbroic rocks have variable contents of SiO₂ (~45–54 wt%), Al₂O₃ (~10–22 wt%), MgO (~4–16 wt%), and CaO (~10–20 wt%), reflecting different extents of fractionation and/or modal contents of olivine, orthopyrox-

ene, clinopyroxene, and plagioclase. Gabbroic rocks are Ti-poor, with ~0.06–0.9 wt% TiO₂; a microgabbro dike within the gabbro cumulate contains more TiO₂ (0.9 wt%). Isotropic gabbros show an island-arc tholeiites (IAT) signature in the Ti versus V diagram (Shervais, 1982) (Fig. 11B). Gabbroic rocks show three distinct patterns of rare earth and other trace elements (Figs. 10A and 10B). Cumulate gabbros have low REE concentrations compared to fine-grained isotropic gabbros and the microgabbro dike. Cumulate gabbros are highly depleted in LREE (La_(n)/Yb_(n) = 0.04–0.23) but with nearly flat REE patterns from HREE to MREE (Gd_(n)/Yb_(n) = 0.7–1.2). Eu enrichment is also noticeable. Extreme depletion in Nb, Ta, and Zr (e.g., Nb_(n)/La_(n) = 0.05–0.2) and enrichment in U, Pb, Ba, and Sr (e.g., Sr_(n)/La_(n) = 93–338) relative to LREE is characteristic of these rocks (Fig. 10B).

Isotropic gabbros are enriched in bulk REE compared to the cumulate gabbros and show LREE-depletion to almost flat patterns (La_(n)/Yb_(n) = 0.3–0.7). These rocks are slightly depleted in Nb and Zr (e.g., Nb_(n)/La_(n) = 0.3–0.9) and enriched in Sr, Th, and U (Fig. 10B). The microgabbro dike shows a flat REE pattern (La_(n)/Yb_(n) = 1.2), weak negative anomalies in Nb-Ta and enrichment in Sr, Th, U, Ba, and Rb.

Crustal Rocks

The Torbat-e-Heydarieh massive lavas have similar contents of SiO₂ (~47–49 wt%), TiO₂ (1.1–1.6 wt%), and Mg# (100Mg/Mg + Fe⁺²) (54–63) (Supplementary Table DR4; see footnote 1). Pillow lavas show greater variability, ranging from 49 to 55 wt% SiO₂, Mg# values of 33–60, and TiO₂ contents of 0.4–2.4 wt%. These volcanic rocks exhibit both tholeiitic and calc-alkaline tendencies in the FeO/MgO versus SiO₂ diagram

¹IGSA Data Repository item 2019304, electronic Appendix A and Supplementary Tables DR1–DR8, is available at <http://www.geosociety.org/datarepository/2019> or by request to editing@geosociety.org.

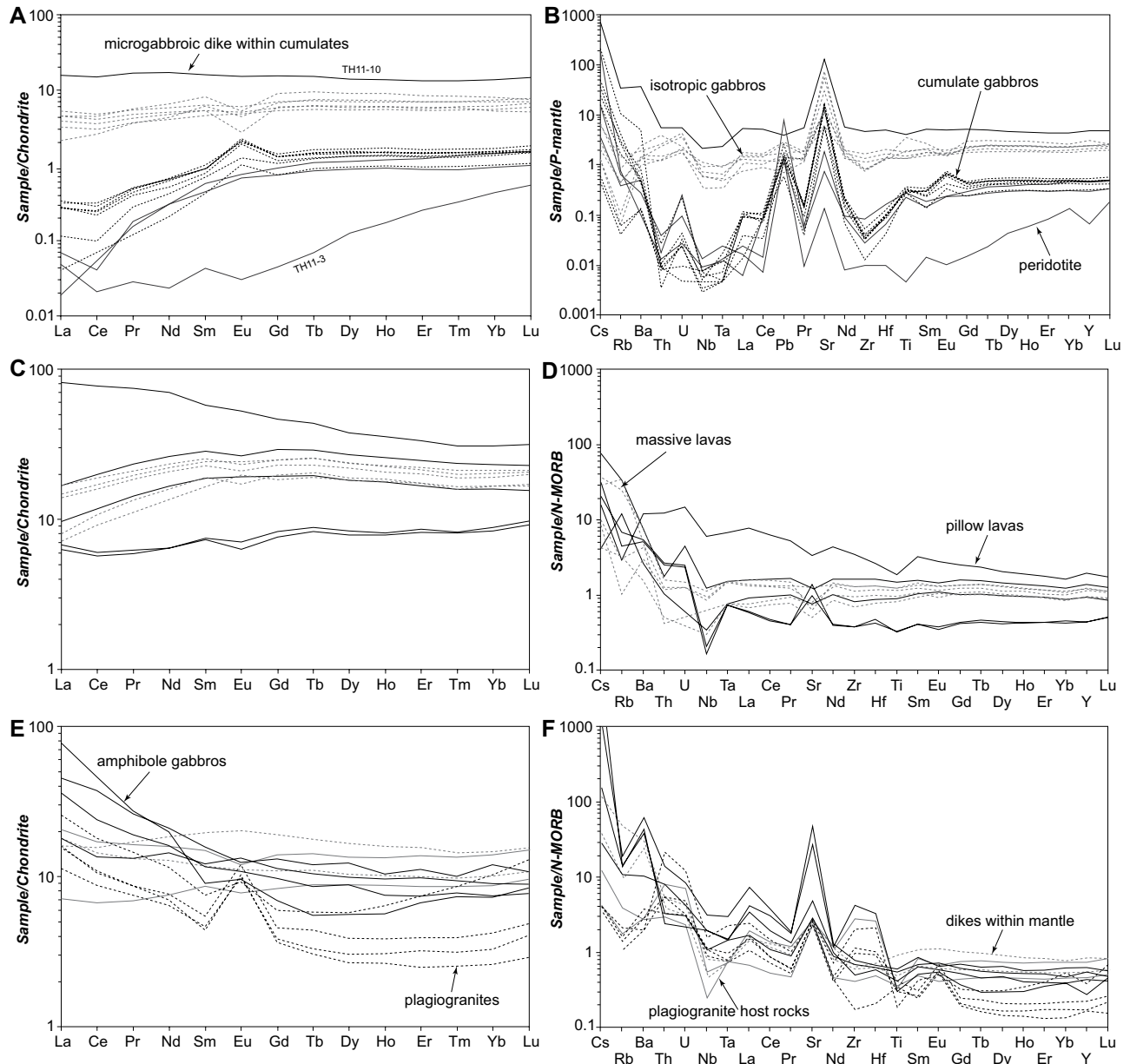


Figure 10. (A–F) Chondrite-normalized rare earth element patterns (chondritic abundances from McDonough and Sun (1995) and primary mantle (P-mantle) and normal mid-ocean-ridge basalt (N-MORB) normalized multi-element patterns (N-MORB and primary mantle concentrations from McDonough and Sun, 1995) for Torbat-e-Heydarieh peridotites, mantle gabbros, plagiogranites, and crustal magmatic rocks.

(Miyashiro, 1974) (Fig. 11A). In a Ti versus V diagram (Shervais, 1982), THO volcanic rocks tend to plot in both the IAT and MORB fields. Sample TH11-39 shows affinity to enriched E-type MORB (E-MORB)-type lavas (Fig. 11B).

Massive lavas are depleted in LREE relative to HREE ($La_{(n)}/Yb_{(n)} = 0.5–0.8$) and have a slight to moderate depletion in Nb ($Nb_{(n)}/La_{(n)} = 0.4–0.7$). They are not enriched in Ba, Th, or U ($Th_{(n)}/La_{(n)} = 0.7–1$) relative to normal mid-ocean-ridge basalt (N-MORB) (Figs. 10C, 10D). These characteristics are similar to

back-arc basin basalts or early arc tholeiites (Peate and Pearce, 1998). These lavas differ from Sabzevar calc-alkaline lavas, which are enriched in LREE, Th, U, and extremely depleted in Nb (Moghadam et al., 2014a).

Pillow lavas can show both enrichment and depletion in LREE relative to HREE ($La_{(n)}/Yb_{(n)} \sim 0.6–2.7$) as well as variable Nb-Ta depletion and Th enrichment (e.g., $Nb_{(n)}/La_{(n)} = 0.3–0.8$ and $Th_{(n)}/La_{(n)} = 1.2–4.3$) relative to N-MORB (Figs. 10C, 10D). They are geochemically similar to E-MORB and depleted

tholeiitic lavas. There is no clear relationship between these two types of pillow lavas in the field.

Plagiogranites and Their Host Rocks

Plagiogranites and their host rocks (diorites and diabasic dikes) have variable SiO_2 (71–79 wt% for plagiogranites and 56–58 wt% SiO_2 for host rocks) and TiO_2 (0.2–0.5 wt%) contents (Supplementary Table DR4). Plagiogranites and their host rocks have LREE-enriched and flat REE patterns respectively

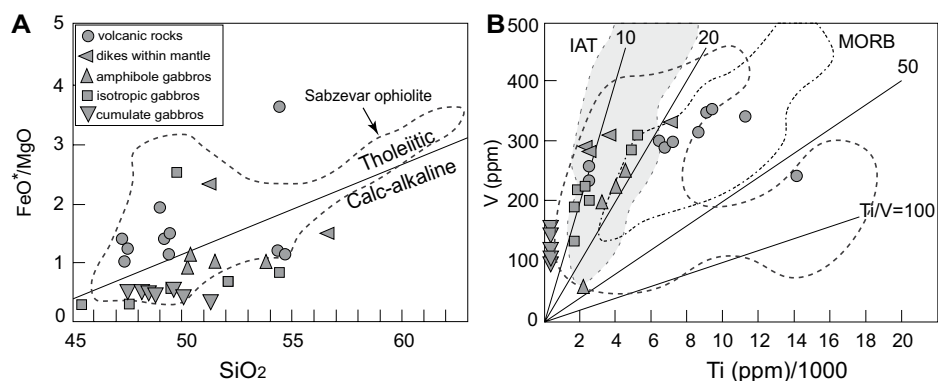


Figure 11. (A) FeO*/MgO vs. SiO₂ (Miyashiro, 1974) and (B) Ti vs. V diagrams (Shervais, 1982) for Torbat-e-Heydariyeh ophiolite rocks. Data for the Sabzevar ophiolite are from (Moghadam et al., 2014a).

(La_(n)/Yb_(n) = 0.8–3.7) with depleted Nb and Ta contents (Nb_(n)/La_(n) = 0.3–0.9) accompanied by Ba, U, K, and Th enrichment (Th_(n)/La_(n) ~ 2–9) relative to N-MORB (Fig. 10F). Plagiogranites also show strong positive anomalies in Sr and sometimes in Eu. These geochemical features are similar to Sabzevar plagiogranites (Moghadam et al., 2014a) and felsic igneous rocks of convergent plate margins (Pearce et al., 1984). These geochemical signatures are also similar to the geochemical characteristics of plagiogranites from other Tethyan ophiolites of the eastern Mediterranean realm (e.g., Anenburg et al., 2015; Bonev and Stampfli, 2009; Dilek and Thy, 2006; Osozawa et al., 2012; Üner et al., 2014).

Mantle Dikes

Diabasic and dioritic dikes injected into mantle peridotites have SiO₂ ~ 50–57 wt%, with Mg# ranging between 43 and 82 (Supplementary Table DR4). Their TiO₂ contents are low, ranging from 0.1 to 1.2 wt%. In the FeO*/MgO versus SiO₂ diagram, the dikes are broadly calc-alkaline, excluding sample TH11-19 (Fig. 11A). In a Ti versus V diagram (Shervais, 1982), these rocks plot in the IAT field (Fig. 11B). Diabasic dikes are characterized by flat REE patterns (La_(n)/Yb_(n) = 1.1–1.8), depletions in Nb and Ta (Nb_(n)/La_(n) = 0.3–0.5), and Ba, U, Sr, and Th enrichment (Th_(n)/La_(n) = 2.6–3.2), resembling IATs. Amphibole gabbros are characterized by an IAT signature in the Ti versus V diagram (Fig. 11B). They show LREE-enriched concave-upward patterns (La_(n)/Yb_(n) ~ 2–10) and depletion in Nb and Ta (Nb_(n)/La_(n) ~ 0.4–0.6).

MINERAL COMPOSITION

Major element compositions of the main rock-forming minerals were determined in

mantle peridotites and cumulate gabbroic rocks: olivine, spinel, orthopyroxene, clinopyroxene, plagioclase, and amphibole. Trace-element contents of clinopyroxenes are also presented. These results are discussed below.

Olivine

Olivine in dunite has forsterite contents ranging from 92.8% to 93.1% (Fo_{92.8–93.1}) with high NiO content (~0.3–0.4 wt%) (Supplementary Table DR1), typical for mantle olivine. Olivine in the harzburgites and Cpx-harzburgites is slightly less magnesian (but still mantle-like) with Mg# and NiO between 91.4 and 91.9 (Fo_{91.4–91.9}) and 0.34–0.43 wt%, respectively. Lherzolites and impregnated lherzolites are characterized by olivine Mg# and NiO content of 89.5–91.3 (Fo_{89.5–91.3}) and 0.34–0.52 wt% respectively, also mantle-like. Olivine in plagioclase lherzolites has lower Fo and NiO contents (Fo_{84.8–85.6} and 0.18–0.24 wt%) than commonly are found in mantle peridotite. These olivines have a magmatic composition (compared to high Mg# mantle olivines) and are interpreted to have crystallized from impregnating mafic melts.

Spinel

Peridotite spinels show variable Cr# (100Cr/(Cr + Al); 10–63), similar to those in abyssal, back-arc basin, and fore-arc peridotites (Dick and Bullen, 1984) (Fig. 12). Spinel from dunites has higher Cr# (59–63) and TiO₂ contents (0.18–0.25 wt%) and follows the peridotite-boninitic melt interaction trend of (Pearce et al., 2000a) (Figs. 12A, 12B). Spinel from harzburgites and Cpx-harzburgites have variable contents of TiO₂ (0.03–0.07 wt% in harzburgites and 0.1 to ~0.3 in Cpx-harzburgites) and FeO (~12.2–12.8 wt% in harzburgites and 14.2–15.5 wt% in Cpx-harzburgites). Harzburgite spinels have lower Cr# (22–24) than Cpx-harzburgite spinels (24–36).

gite spinels have lower Cr# (22–24) than Cpx-harzburgite spinels (24–36).

Spinel of lherzolites and impregnated lherzolites have variable contents of TiO₂ (0.02–0.12 wt%) and Cr# (10–20). Spinel compositions of lherzolites and impregnated lherzolites overlap at low Cr#. This is because these two rocks have similar mineral assemblages; impregnated lherzolites have more coarse-grained clinopyroxene aggregates with the lightest brown spinels. The Cr# of their spinels is similar to that of abyssal peridotites (Dick and Bullen, 1984). Spinel from plagioclase lherzolites have high TiO₂ (0.15–0.25 wt%) and FeO (~31–39 wt%) content and high Cr# (41–48).

Orthopyroxene

Orthopyroxene in harzburgite and Cpx-harzburgite has high Mg# (91–92) and elevated contents of Al₂O₃ (2.7–5 wt%) and Cr₂O₃ (0.56–1 wt%) (Supplementary Table DR1). Orthopyroxene in lherzolites and impregnated lherzolites has constant Mg# (89–91) but variable Al₂O₃ (~3–6.1 wt%) content. Plagioclase-lherzolite orthopyroxenes have low Mg# (86) and Al₂O₃ (2.1–2.3 wt%) compared to orthopyroxene from other THO peridotites. Orthopyroxene in gabbros has lower Mg# (79–84) and Al₂O₃ contents (1.5–2.1 wt%). The Al₂O₃ content of the THO peridotite orthopyroxenes are relatively high, ranging from 1.5 to 6.1 wt%; the higher values are encountered in impregnated lherzolites. However, the Al₂O₃ content of orthopyroxene from fertile spinel peridotites from ophiolites in other worldwide localities (e.g., the Vardar ophiolite [Bazylev et al., 2009], and fertile peridotites from the Yarlung Zangbo suture zone [Bédard et al., 2009]) and oceanic back-arcs (e.g., Mariana Trough [Ohara et al., 2002], and South Sandwich arc-basin [Pearce et al., 2000b]) are also high, resembling the THO impregnated lherzolites, and show the fertile nature of the host mantle rocks.

Clinopyroxene

Clinopyroxene is abundant in dunite as inclusions in large chromites. Its composition is Wo_{49–51}En_{47–49}Fs_{2–3}. It has high Mg# (94–97) and low TiO₂ (0.06–0.19 wt%) and Al₂O₃ (0.6–~2 wt%). Harzburgites and Cpx-harzburgites contain clinopyroxene with Wo_{44–52}En_{48–49}Fs_{3–4}. Clinopyroxene in Cpx-harzburgites have higher TiO₂ (0.26–0.35 wt%), but lower Al₂O₃ (3.9–4.6 wt%) compared to those in harzburgites (TiO₂ = 0.12–0.17 wt%; Al₂O₃ = 3–5.2 wt%) (Fig. 12C) with identical Mg# (92–94). Clinopyroxene in mantle lherzolites and impregnated lherzolites has variable composition (Wo_{36–51}En_{45–59}Fs_{4–6}) with high Mg# (91–93), Al₂O₃

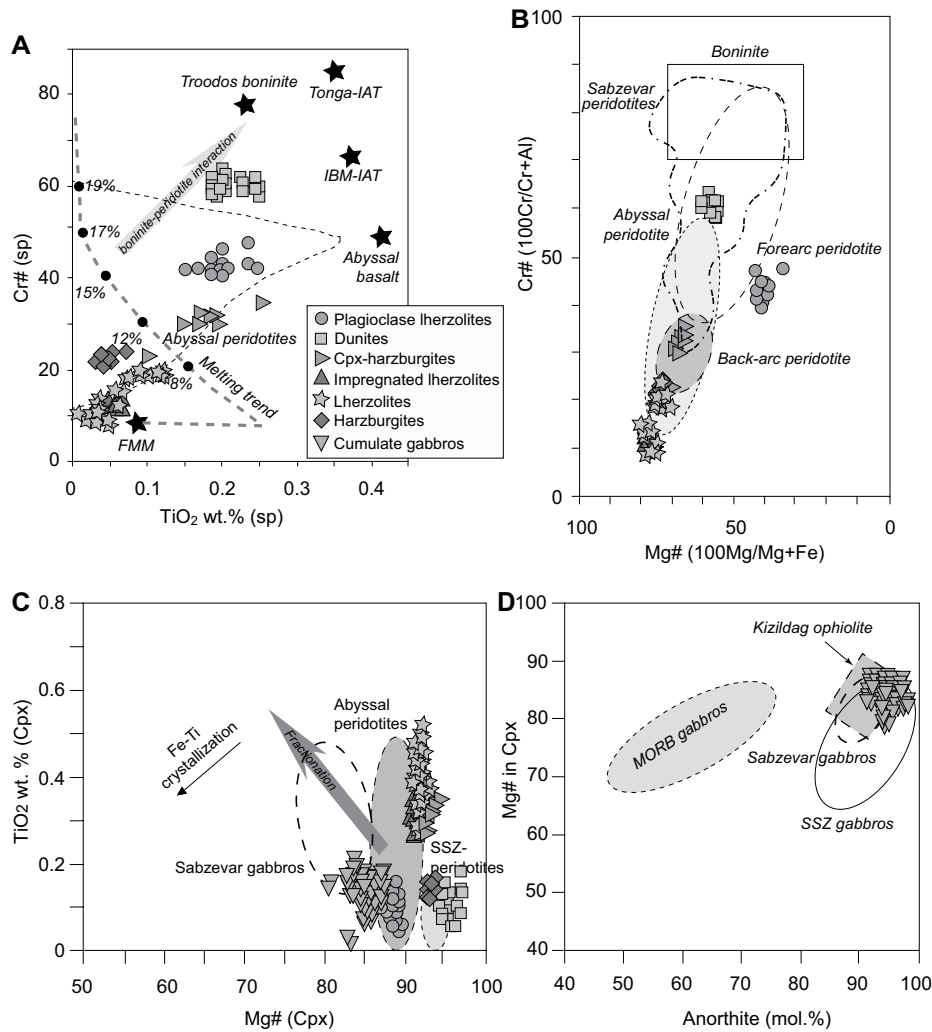


Figure 12. (A) Relationship between Cr# and TiO₂ contents of spinel in mantle peridotites of the Torbat-e-Heydarieh ophiolite. The thick gray arrow shows the effect of melts (with composition of Troodos boninites) on refractory subduction-zone peridotites. Compositions of Tonga and Izu-Bonin-Mariana island arc tholeiites and abyssal basalts are from (Pearce et al., 2000a) and the composition of Troodos boninite is from (Dick and Bullen, 1984). (B) Relationship between Cr# and Mg# of spinels in Torbat-e-Heydarieh mantle peridotites. Abyssal-peridotite fields are from (Dick and Bullen, 1984), fore-arc-peridotite field is from (Pearce et al., 2000a). Data on Sabzevar peridotites are from (Moghadam et al., 2014a). (C) Mg# vs. TiO₂ contents of clinopyroxene from peridotite and mantle gabbro (abyssal and fore-arc peridotite fields are from (Bédard et al., 2009)). (D) Anorthite content vs. clinopyroxene Mg# (modified after (Sanfilippo et al., 2013) in Torbat-e-Heydarieh gabbroic rocks. The Kizildag ophiolite data are from (Bağcı et al., 2005). Fields of mid-ocean-ridge basalt (MORB) and arc gabbro are from (Burns, 1985). SSZ—supra-subduction zone.

(4.9–7.1 wt%) and TiO₂ (0.3–0.5 wt%) (Supplementary Table DR1). Plagioclase lherzolites have clinopyroxene with more constant composition (Wo_{41–48}En_{46–52}Fs_{6–7}) but with low TiO₂ (0.06–0.16 wt%) and Al₂O₃ (2.2–3.8 wt%) and lower Mg# (87–89) compared to clinopyroxene from other THO lherzolites. On a TiO₂ versus Mg# diagram (Fig. 12C) clinopyroxenes from THO peridotites are similar to those found in both abyssal and SSZ peridotites. Clinopyrox-

ene and spinel from nearly all mantle units of Tethyan ophiolites show both abyssal and SSZ geochemical signatures (e.g., Aldanmaz, 2012; Ghazi et al., 2010; Monsef et al., 2010). This geochemical duality can be also observed in the crustal lavas of Neotethyan ophiolites (e.g., Dilek and Furnes, 2009; Dilek et al., 2007; V).

Clinopyroxene in gabbro has variable composition (Wo_{37–47}En_{45–51}Fs_{7–13}). The more evolved compositions (with low Ca but high Fe) are

found in smaller crystals between large clinopyroxenes. Gabbroic clinopyroxenes have TiO₂ and Al₂O₃ contents from 0.07 to 0.21 and 1.7–2.8 wt%, respectively; these are lower than in Sabzevar gabbroic clinopyroxenes.

Plagioclase

Plagioclase in plagioclase lherzolites is highly altered; unaltered portions show very high An contents (96.2%–98.3%). Gabbro plagioclase is also anorthite-rich (~An 91.1–98.2) (Supplementary Table DR1); amphibole-bearing gabbros with less orthopyroxene contain An_{91–92} plagioclase. Comparison of the clinopyroxene Mg# against anorthite content in plagioclase (Sanfilippo et al., 2013), shows a pattern similar to SSZ-type gabbros (Fig. 12D).

Amphibole

Analyses of amphibole inclusions within dunite chromites, plotted in the Mg# versus Si diagram (not shown), show that these are pargasite to edenite according to Leake et al. (1997). The Cr₂O₃ contents of these amphiboles are high (2.4–3.1 wt%).

Clinopyroxene: Trace-Element Geochemistry

Trace-element abundances (including REEs) in THO lherzolites, impregnated lherzolites, plagioclase lherzolites, and cumulate gabbros are listed in Supplementary Table DR2 (see footnote 1).

All mantle clinopyroxenes from the THO are enriched in REEs with LREE-depleted patterns. They are similar to REE abundances in Cpx from mid-ocean ridge (MOR) cumulates and abyssal peridotites and are much more enriched than those in SSZ peridotites (Figs. 13A, 13C).

Chondrite-normalized REE patterns of clinopyroxenes from THO lherzolites are strongly depleted in light REEs (LREE) but are flat in middle to heavy REEs (MREE–HREE). These patterns are similar to those of Cpx in oceanic abyssal peridotites (Bizimis et al., 2000; Johnson et al., 1990), although total REE concentrations are greater (Fig. 11A). The REE content of THO lherzolite Cpx is even higher than Cpx from Sabzevar plagioclase lherzolites (Fig. 13B) (Shafaii Moghadam et al., 2015). Clinopyroxene trace-element patterns are depleted in Ti and Zr, but not in Sr and Eu (Fig. 13B). Clinopyroxene in THO impregnated lherzolites exhibits REE patterns similar to Cpx from THO lherzolites, characterized by higher total REE contents compared to Cpx from abyssal peridotites and

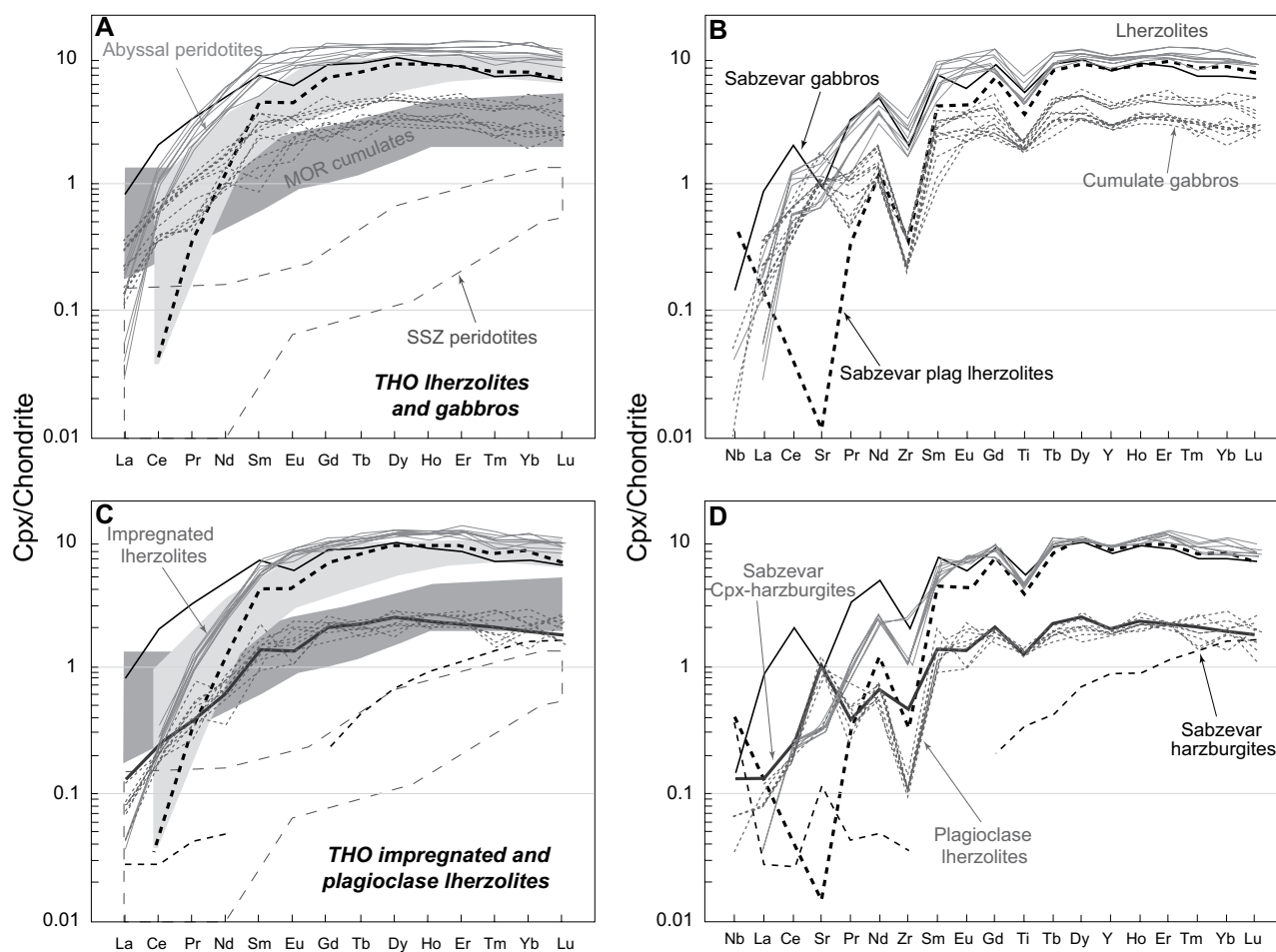


Figure 13. Abundances of rare earth elements and other trace elements in clinopyroxene in lherzolites and cumulate gabbros (A, B) and impregnated and plagioclase lherzolites (C, D), from the Torbat-e-Heydarieh ophiolite (THO). Chondrite normalization values are from McDonough and Sun (1995). Fields for abyssal and supra-subduction zone (SSZ)–peridotite clinopyroxenes are from Bizimis et al. (2000) and Johnson et al. (1990). The composition of mid-ocean-ridge cumulate clinopyroxene (Cpx) is from Ross and Elthon (1993). Data on Sabzevar ophiolite rocks are from Shafaii Moghadam et al. (2015).

Sabzevar lherzolites (Fig. 13C). Negative anomalies in Ti and Zr are also obvious (Fig. 13D).

Cpx in THO plagioclase lherzolites have REE patterns similar to those of Cpx from MOR cumulates (Ross and Elthon, 1993), but with more depleted LREE (La–Sm, Fig. 13C). These patterns are also similar to those for Cpx from Sabzevar Cpx-harzburgites. MREE–HREE abundances in Cpx of plagioclase lherzolite are depleted compared to Cpx from THO lherzolites and impregnated lherzolites (Fig. 13C). Slight depletion in Ti and strong Zr negative anomalies are conspicuous in plagioclase lherzolites (Fig. 13D).

The REE abundances and patterns of clinopyroxenes in THO gabbro cumulates are in the range of those exhibited by MOR cumulates (Ross and Elthon, 1993) (Fig. 13A), but with more convex-upward MREEs with Sm–Ho peaks. They are similar to clinopyroxene patterns from Sabzevar cumulate gabbros but with

lower REE abundances (Fig. 13A). The Cpx from cumulate gabbros are depleted in Zr and Ti but enriched in Sr (Fig. 13B). Trace-element patterns of Cpx in cumulate gabbros are between those from Cpx of plagioclase and impregnated lherzolites.

Nd–Hf Isotopes

Eight samples were selected including depleted tholeiitic pillow lavas, back-arc basin-type massive lavas, SSZ-type plagiogranites, IAT-like diabasic dike and back-arc– to fore-arc–type gabbros for analysis of whole-rock Nd and Hf isotopes. Hf–Nd isotope compositions are useful for inferring mantle source characteristics and the role of sediments and older continental crust in generating subduction-related magmas (Vervoort and Blichert-Toft, 1999b; Vervoort et al., 1999; Woodhead et al., 2012; Yagodinski et al., 2010).

The $\epsilon_{\text{Nd}}(t)$ and $\epsilon_{\text{Hf}}(t)$ values for THO rocks vary between +5.7 to +8.2 and +14.9 to +21.5 respectively; gabbro shows especially high $\epsilon_{\text{Hf}}(t)$ (+21.5) (Fig. 14A). All the samples plot near the field for modern Indian Ocean MORBs, suggesting a similar mantle source (Chauvel and Blichert-Toft, 2001b). Figure 13B shows the results of bulk-mixing calculations between mantle-derived MORB melts and various types of sediments (Chauvel et al., 2009). Involvement of subducted Fe–Mn rich sediments (as well as calcareous clays) in the mantle source affects Nd– more than Hf isotopic compositions (Fig. 14B). In contrast, addition of continental sands will affect Hf as well as Nd isotopic compositions, depending upon whether bulk assimilation of sediments or sediment melts are involved. Also, the different Hf/Nd ratios of sediments are expected to have a large influence, especially with the contribution of zircons in the subducted sediments.

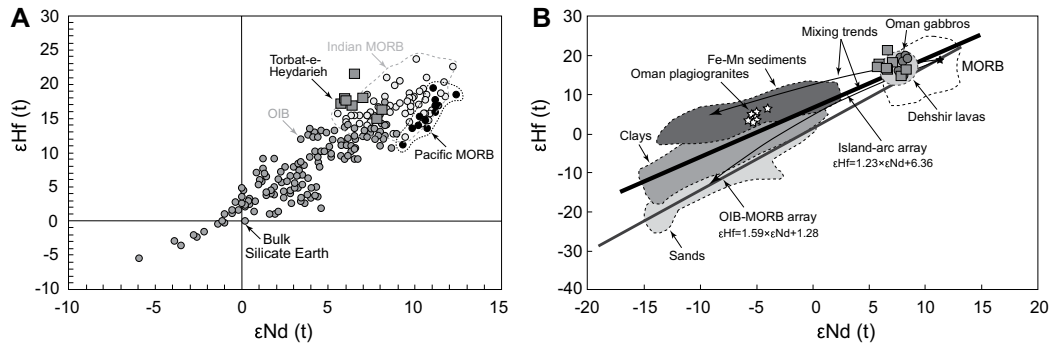


Figure 14. ϵHf vs. ϵNd for the Torbat-e-Heydarieh magmatic rocks, recalculated at 100 Ma (modified after Chauvel et al., 2009). In (A), our samples are compared to the mid-ocean-ridge basalt (MORB) and ocean-island basalt (OIB)-type lavas, whereas in (B), the mixing trend between depleted mantle reservoir and different types of sediments is shown. Data for Oman plagiogranites are from Haase et al. (2015) and data from Dehshir ophiolites are from Moghadam et al. (2012). MORB and OIB data are from Chauvel and Blichert-Toft (2001a), Nowell et al. (1998), Pearce et al. (1999), and Woodhead et al. (2001). Mantle array data are after Vervoort and Blichert-Toft (1999a).

In contrast to the Oman plagiogranites, which show strong involvement of sediment melts in their magmatic reservoir (Haase et al., 2015), the mantle sources of the Torbat-e-Heydarieh plagiogranites were not significantly affected by sediment melt addition or crustal assimilation. However, the mantle source of the Torbat-e-Heydarieh magmatic rocks could have been slightly affected by subducted pelagic sediments (high Nd/Hf ratio), because they vary considerably in $\epsilon\text{Nd}(t)$. They have less radiogenic Nd- isotope compositions than the igneous rocks of the Dehshir Late Cretaceous ophiolite (inner belt Zagros ophiolites; Fig. 1; Moghadam et al., 2010). The Nd-isotope compositions of the THO magmatic rocks are similar to those of the Sabzevar ophiolite from NE Iran, which have high but variable $\epsilon\text{Nd}(t)$ values (+5.4 to +8.3) and moderately high $^{207}\text{Pb}/^{204}\text{Pb}$ ratios (15.50–15.65) (Moghadam et al., 2014a). The Nd-Hf-Pb isotopic compositions of the Sabzevar-Torbat-e-Heydarieh rocks suggest a minor contribution of subducted sediments to the mantle source of these ophiolites from NE Iran.

ZIRCON GEOCHRONOLOGY

Four plagiogranites and two diabasic and gabbroic mantle-intruding dikes from the THO have been dated. We also analyzed five of these zircon separates for Hf-isotope compositions.

Sample TH11-23

This sample is taken from a plagiogranitic dike injected into the mantle diabasic dikes. Zircons are euhedral and prismatic and show

magmatic concentric zoning (Fig. 15). These zircons contain 215–762 ppm U and have high Th/U ratios of 0.6–1.7 (Supplementary Table DR6; see footnote 1), consistent with a magmatic origin. Twenty-one analyses define a mean $^{206}\text{Pb}/^{238}\text{U}$ age of 99.32 ± 0.72 Ma (MSWD = 1.4) (Fig. 15). This is interpreted as the time of plagiogranite crystallization. Zircons from this sample show a wide range of $\epsilon\text{Hf}(t)$, between $-+8$ and $+16.1$ (Supplementary Table DR8; see footnote 1).

Sample TH11-12

This sample is taken from a rodingitized gabbroic dike injected into mantle peridotites. The Th/U ratio of analyzed zircons varies between 0.47 and 0.69, consistent with a magmatic origin. Six analyzed grains yield a mean $^{206}\text{Pb}/^{238}\text{U}$ age of 96.7 ± 2.1 Ma (MSWD = 0.32) (Fig. 15). This is the age of gabbroic dike intrusion and provides a minimum age for the THO formation. Zircons from this sample show $\epsilon\text{Hf}(t)$ values that vary from $-+9$ to $+16.9$.

Sample TH11-82B

This plagiogranite intrudes mantle cumulate gabbros. Twenty-five zircons from this sample were dated by LA-ICPMS. Cathodoluminescence (CL) images show that the grains are medium-grained ($<100 \mu\text{m}$) and euhedral to subhedral (Fig. 15). Zircons have low to medium U (25–420 ppm) and Th (10–208 ppm) concentrations, and Th/U ratios vary between 0.4 and 0.7 (Supplementary Table DR7; see footnote 1), consistent with a magmatic origin. The $^{206}\text{Pb}/^{238}\text{U}$ and $^{207}\text{Pb}/^{235}\text{U}$ data define a con-

cordia age of 91.9 ± 0.33 Ma (MSWD = 1.7). This is interpreted as the age of plagiogranite crystallization. Zircons from this sample show $\epsilon\text{Hf}(t)$ values of $-+9.8$ to $+15.1$ (Supplementary Table DR8).

Sample TH11-74

This plagiogranite intrudes mantle cumulate gabbros. We analyzed 14 zircons from this sample. CL images indicate magmatic zonation. Zircons have low to medium U (53–613 ppm) and Th (26–364 ppm) concentrations, and Th/U ratios vary between 0.5 and 1.3 (Supplementary Table DR7). In the concordia diagram, 14 analyses yield an age of 97.0 ± 1.3 (MSWD = 0.2) (Fig. 15). Zircons from this sample show $\epsilon\text{Hf}(t)$ values that vary from $-+11.3$ to $+17.6$.

Sample TH11-29

This sample is a diabasic dike within the mantle peridotites and contained only eight zircons. Zircons from this sample are prismatic ($\sim 50 \mu\text{m}$ to $\sim 100 \mu\text{m}$). CL images show oscillatory zoning in some grains and some are less luminescent with weak zonation. Eight analyzed spots have high Th/U values (0.3–1.6). Five of the analyzed zircons show concordant ages with weighted mean of $^{206}\text{Pb}/^{238}\text{U}$ age of 97.1 ± 1.2 (MSWD = 0.6) (Fig. 15). The striking feature of this sample is the presence of three xenocrystic zircons with $^{207}\text{Pb}/^{235}\text{U}$ ages of ~ 1.1 – 1.5 Ga. Late Cretaceous zircons from this sample show $\epsilon\text{Hf}(t)$ values that vary from $-+8.1$ to $+12.7$, whereas the old zircons have $\epsilon\text{Hf}(t)$ values between $+1.7$ and $+6.2$ (Supplementary Table DR8).

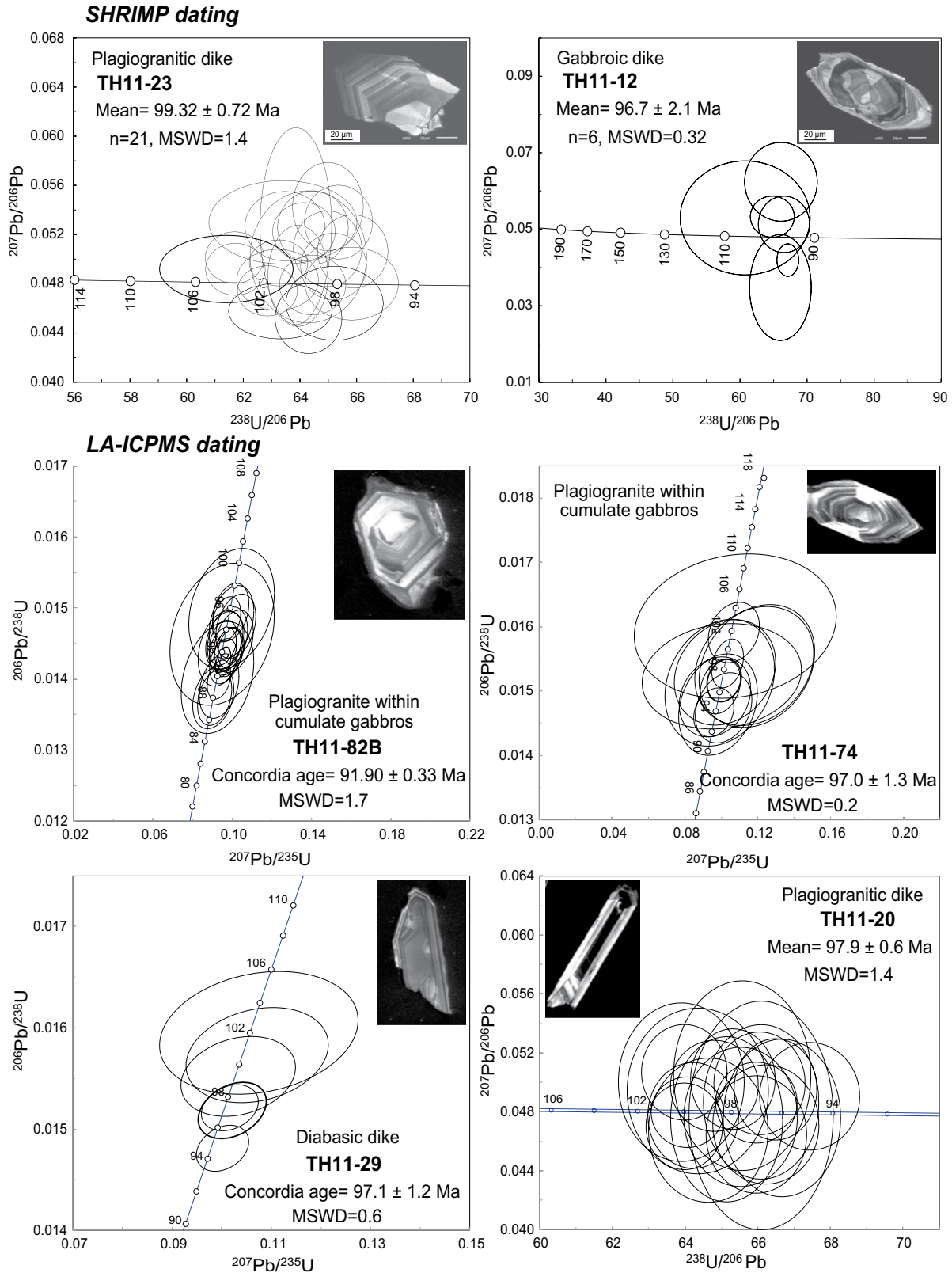


Figure 15. Zircon sensitive high-resolution ion microprobe (SHRIMP) and laser ablation–inductively coupled plasma mass spectrometry (LA-ICPMS) U–Pb data from the Torbat-e-Heydarieh plagiogranite and diabasic-gabbroic dikes. MSWD—mean square of weighted deviates.

Sample TH11-20

Zircon grains from this sample, a plagiogranitic dike within the crustal gabbros, are long-prismatic and euhedral. Most crystals have magmatic zonation. Twenty-five analyses show low to moderate Th/U (~0.2–0.7) (Supplementary Table DR7). Analyses are concordant, yielding a weighted mean age of 97.9 ± 0.6 Ma (MSWD = 1.4). This is interpreted as the crystallization age for this dike. Zircons from this sample show $\epsilon\text{Hf}(t)$ values that vary from -13 to $+18.5$.

DISCUSSION

This new geochemical and isotopic data set from the THOs allows a detailed investigation of the mantle characteristics and the source of crustal rocks; the timing of back-arc basin opening and the relationship of this ophiolite to other Iranian ophiolites; the tectonic setting in which the THO formed; and the implications for understanding Late Cretaceous tectonic evolution in the region.

Sources of Mantle Peridotites and Crustal Melts

Mineral and whole-rock compositions of various mantle peridotites, crustal gabbros, and effusive lavas classify the rocks into four different tectonic settings: abyssal peridotite, SSZ fore-arc (FA), island-arc (IA), and back-arc basin (BAB) settings.

Mantle Peridotites of Mid-Ocean-Ridge Origin

Iherzolites and impregnated Iherzolites show affinities with abyssal (MOR) peridotites. Compositions of Cr-spinel and co-existing olivine all plot in a confined field between fertile MORB-source mantle and its partial melts (Figs. 9A, 9B). The clinopyroxene and spinel compositions of impregnated Iherzolites are similar to the mineral compositions of Iherzolites, suggesting these phases precipitated from the same melts during the impregnation. The overall compositional trends show mixing between a fertile MORB-source mantle source and its partial melting residue ($F = \sim 9\%$). The trend may also represent various degrees of extraction (Iherzolite) and addition (impregnated Iherzolite) of basaltic melts (Fig. 10A). Clinopyroxene compositions in these rocks also plot within the enriched part ($\text{TiO}_2 > 0.2$ wt%) of the abyssal-peridotite field (Fig. 10C). Such variations can form in the fractional to reactive melting regime in the spinel-stability field beneath a spreading ridge (Kimura and Sano,

2012), as envisaged by the clinopyroxene REE patterns with flat MREE to HREE and depleted LREE (Figs. 10A–10C).

Dunite of Supra-Subduction Zone Fore-arc Origin

Spinel in dunite samples are rich in Cr and Ti and their compositions plot close to the boninite and IAT basalt field (Figs. 9A, 9B). They plot away from the abyssal peridotite field, into the SSZ field. Because of the proximity of the compositions of spinel and clinopyroxene to those of boninite or IAT, these are most like SSZ fore-arc peridotites.

Plagioclase Iherzolite and Cumulate Gabbro of Supra-Subduction Zone–Island-arc Origin

Cumulate gabbros contain low-Mg# clinopyroxene and An-rich (~90%) plagioclase. These are features of assemblages formed from water-rich arc basalt magmas (e.g., Hamada and Fujii, 2008). Therefore, the gabbros are most similar to arc magmas (Ishizuka et al., 2014).

Spinel in plagioclase Iherzolites show intermediate abundances of Cr and Ti (Figs. 9A, 9B). Clinopyroxenes have low Mg# and are poor in Ti, similar to cumulate gabbros. The low-Ti content of clinopyroxenes from plagioclase Iherzolites suggests crystallization from a SSZ-derived melt during magmatic impregnation. The Cr and Ti compositions of plagioclase Iherzolite spinels lie between the fields of abyssal peridotite and basalt (Fig. 10A); however, Mg# in the spinel plots away from abyssal peridotite but close to SSZ-FA peridotite. Considering the Mg#-rich spinel and Mg-poor clinopyroxene together (Figs. 9B, 9C), the plagioclase Iherzolites suggest affinities with island-arc tholeiites.

The REE patterns of clinopyroxenes from cumulate gabbros show depleted MREE to HREE relative to MOR gabbros with elevated Sr (Fig. 11B). Plagioclase Iherzolites show the same feature, with more depleted MREE to HREE and elevated Sr (Fig. 11D). Low REE abundance is the signature of a depleted mantle source and elevated Sr may reflect addition of metasomatic slab-derived fluid. Sr enrichment in plagioclase-bearing peridotites is also suggested to postdate melt impregnation and could be the result of high-temperature (370–850 °C) breakdown of plagioclase, which liberated Sr to enrich adjacent pyroxenes (Pirnia et al., 2014).

The lower abundances of Zr in plagioclase Iherzolites relative to Iherzolites and depletion of high field strength elements in the mantle and gabbro sources are consistent with hydrous metasomatism (Arai et al., 2006; Khedr and Arai, 2009). This feature is most consistent with a SSZ-FA origin of the mantle-crust lithologies.

Harzburgite and Cpx-Harzburgite of Back-arc Basin Origin

Spinel in harzburgite have intermediate Mg# (66–76) and partially overlap Iherzolite fields (Figs. 9A, 9B). In contrast, spinels with lower Ti and higher Cr than those of Iherzolite are more depleted (Figs. 9A, 9B). Ti contents are low in both clinopyroxenes and dunite, suggesting a SSZ signature (Fig. 10C). Any further constraints on harzburgite tectonic affinities are difficult to identify.

Cpx-harzburgite forms common geochemical trends with harzburgite. They plot between abyssal basalt, abyssal peridotite, and SSZ dunite (Figs. 9A–9C). The depleted nature of these rocks implies that harzburgite was impregnated by MORB or IAT melt (Figs. 9A–9C). It is difficult to identify the impregnated melts as either MOR or IA. The harzburgites, however, are distinct from abyssal peridotites suggesting involvement of strongly depleted mantle ($F = \sim 12\%$; Fig. 9A). Such highly depleted sources can occur in fore-arc or BAB settings (Hirahara et al., 2015). We thus conclude that harzburgite and cpx-harzburgite probably formed in a fore-arc or back-arc basin.

No Cpx-REE data are available for the Cpx-harzburgites. Some insight may be gained by considering harzburgite clinopyroxenes from the nearby Sabzevar ophiolite. These are extremely depleted (Fig. 11D) consistent with a SSZ mantle origin of the NE Iran ophiolite harzburgites and impregnated harzburgites.

Isotropic and Cumulate Gabbros: Back-arc Basin or Fore-arc Origin?

Isotropic gabbros show flat to slightly LREE-depleted patterns with lower total abundances than N-MORB, along with Nb-Ta troughs and elevated La and Th (Fig. 12B). These geochemical features are close to those of fore-arc basin from the Izu-Bonin-Mariana fore-arc (Reagan et al., 2010), although Nb-Ta depletions are greater in THO rocks. One microgabbroic dike is similar, with more elevated trace-element abundances and no Eu anomaly (Figs. 11A, 11B). This may represent a melt-rich part of the gabbros. Although some depleted IA basalts generated during BAB opening show similar trace-element patterns, these are generally richer in Pb, Th, and LREEs (e.g., Shinjo et al., 1999). Similarly, E-MORB erupted in the Sea of Japan back-arc basin during its opening at ca. 17 Ma (Hirahara et al., 2015). Depleted D-type MORB is also associated with the opening of the Sea of Japan (Hirahara et al., 2015). Sea of Japan D-type basalts are geochemically similar to THO isotropic gabbros, apart from depleted HREE due to residual garnet in the source of the former basalts (Hirahara et al., 2015). According to

these considerations, we find that the isotropic gabbros are most similar to FA or BAB.

In contrast to the isotropic gabbros, cumulate gabbros show elevated Sr, Pb, Ba, and Eu anomalies due to plagioclase accumulation. LREE-depleted patterns reflect cumulate clinopyroxene, but the patterns still show Nb-Ta depletion relative to La and Th. This is similar to gabbros of FA or BAB origin. The loss of melt from cumulate gabbros and the concentration of some cumulate minerals could explain the different chemistries of isotropic and cumulate gabbros (Figs. 11A, 11B). Plagioclase is anorthite-rich (Fig. 10D), suggesting that these gabbros most likely originated from water-rich basaltic melts (Hamada and Fujii, 2008). All of the above observations indicate that the THO gabbros are most similar to FA or BAB basalts.

It is hard to specify the tectonic setting of the SSZ gabbros from geochemistry alone; this is consistent with fore-arc, arc, or back-arc basin settings.

Pillow and Massive Basaltic Lavas, Dikes within Mantle of Island-arc–Back-arc Basin Origin

Most lavas show slightly LREE-depleted flat patterns with slight Nb depletion and slight Th enrichment. The pattern is akin to N-MORB, FAB, or BABB. These features are further examined below using Th/Yb and Th/Ce ratios.

A useful observation is the lack of boninite in the THO. Fore-arc volcanic sequences are frequently but not always associated with boninite and high-Mg andesite (Ishizuka et al., 2014; Reagan et al., 2010, for Izu-Bonin-Mariana; Ishikawa et al., 2002, for Oman ophiolite). In the fore-arc setting, boninites are suggested to be generated 2–4 m.y. later than fore-arc basalts, when the residual, highly depleted mantle melted at shallow levels after interaction with a water-rich fluid derived from the subducting slab (Ishizuka et al., 2014; Reagan et al., 2010). However, boninite does not occur in the THO, suggesting that it did not form in a fore-arc subduction-initiation setting.

One pillow-lava sample is enriched in LREE, like E-MORB (Fig. 12D). This sample is similar to OIB-like pillow and massive lavas from the Sabzevar ophiolite (Moghadam et al., 2014a). E-MORB occurs either in MOR or in BAB as an along-ridge geochemical variation (e.g., Kelley et al., 2013). E-MORB also occurred in the SW Japan FA when subduction re-initiated at 15 Ma (Kimura et al., 2005). E-MORB occurs all over MOR-FA-BAB settings, so its presence does not constrain the setting of THO. Melting of enriched subcontinental lithosphere might be responsible for generating THO E-MORB-like lavas.

Two of the most depleted samples have strong Nb depletions and strong Th enrichments (Fig. 12D). REEs are more depleted than MORBs, but with elevated large-ion lithophile elements such as Sr, U, and Ba. These are IAT-like basalts; such basalts occur in BAB and in fore-arcs.

Plagiogranites and Amphibole Gabbros of Island-arc–Back-arc Basin Origin

Plagiogranites and amphibole gabbros all have arc-magma signatures including Nb-Ta troughs and strong Th enrichment (Fig. 12F). HREEs are strongly depleted, similar to IAT-type pillow lavas. LREEs are highly enriched in both lithologies with greater large-ion lithophile element enrichment in amphibole gabbros. Sample TH11-9B geochemically resembles E-MORBs with enriched LREEs and less Nb depletion. Elevated Sr and Eu contents in the plagiogranites are probably due to plagioclase accumulation. Positive Zr-Hf anomalies in the amphibole gabbros and host rocks of plagiogranites are likely to reflect preferential partitioning of these elements into amphibole during fractional crystallization (Tiepolo et al., 2007) (Fig. 12F).

Nb/Yb-Th/Yb Discrimination

Pearce (2008) proposed that Th/Yb versus Nb/Yb relationships could distinguish MORB-OIB from SSZ igneous rocks. Most THO lavas and crustal gabbros show elevated Th/Yb at moderate to low Nb/Yb, consistent with subduction contributions (sediment melt) to a moderately depleted mantle source (Fig. 16A). Exceptions are TH11-70, TH11-33, TH11-32, TH11-64, TH11-67, and TH11-66, which plot along the MORB-OIB array within the N-MORB field, and TH11-39 pillow lava and TH11-9B amphibole gabbro, which plot along the MORB-OIB array within the E-MORB field. Other lavas and gabbros have Nb/Yb similar to N- and E-MORB, but have elevated Th/Yb (Fig. 16A). Pillow and massive lavas, mantle dikes, and cumulate gabbros have low Nb/Yb, whereas amphibole gabbros and plagiogranites show high Nb/Yb indicating derivation of these magmas from more- and less-depleted mantle sources, respectively (Pearce, 2008).

Th/Nb-Ce/Nb Discrimination

Similar conclusions are reached based on the Th/Nb-Ce/Nb plot (Fig. 16B) (Sandeman et al., 2006). Most lava flows (TH11-70, TH11-33, TH11-32, TH11-64, TH11-67, and TH11-66) and the TH11-9A amphibole gabbro have MORB signatures, whereas TH11-39 pillow lava and TH11-9B amphibole gabbro are similar to Sabzevar OIB-type lavas. These are in turn similar to Lau Basin BAB and Okinawa Trough intra-arc rift lavas. In contrast, other IA-BAB-

type lavas, isotropic gabbros, amphibole gabbros, and mantle dikes have lower Ce/Th, plotting close to Okinawa Trough BABs. Overall, THO magmatic rocks including lavas, gabbros, and plagiogranites plot between MORB and Mariana arc lavas, and therefore indicate generation from a heterogeneous depleted MORB mantle source mantle that was variably fluxed by slab fluids.

The above considerations support a BAB origin for the THO magmatic rocks. Only plagiogranites and amphibole gabbros show strong IAT signatures (Fig. 12D). These geochemical signatures resemble Sabzevar ophiolite magmatic rocks (Moghadam et al., 2014a).

Zr/Nb-Hf/Nb and Th/Nd-¹⁴³Nd/¹⁴⁴Nd Discrimination Diagrams

The composition of BAB basalts varies significantly, indicating that BABB melts are derived from heterogeneous mantle sources, which range from depleted to enriched and from MORB-like to arc-like (Stern, 2002; Taylor and Martinez, 2003). The THO igneous rocks are LREE-depleted or slightly enriched relative to N-MORB, similar to BABB (Fig. 12), like those of the Lau Basin (Tian et al., 2011) and Okinawa Trough (Shinjo, 1999). The THO igneous rocks involve both depleted (FAB and D-type BABB-like igneous rocks) and enriched (E-BABB and E-MORB-like rocks) mantle components, a conclusion which is supported by the plot of Hf/Nb versus Zr/Nb (Sorbader et al., 2013) (Fig. 16C).

To better understand the contribution of slab-derived components to the mantle source of THO igneous rocks, we used a plot of Th/Nb versus ¹⁴³Nd/¹⁴⁴Nd (Fig. 16D). THO igneous rocks reflect variable enrichment by sediment melts, as shown on Figure 16D (Sorbader et al., 2013). THO melts are like those of the Sabzevar ophiolite, which sampled multiple mantle and slab components, again consistent with a BAB interpretation.

Whole-Rock Nd-Hf and Zircon Hf Isotopes

Whole-rock ($\epsilon_{\text{Hf}} = +14.9 - +21.5$) and zircon ($\epsilon_{\text{Hf}} = +8.1 - +18.5$) Hf isotope data from the Torbat-e-Heydarieh ophiolite are comparable. These data indicate that the mantle source beneath the THO back-arc was broadly MORB-like (Todd et al., 2011; Woodhead et al., 2012; Woodhead and Devey, 1993). However, this mantle source also had slightly enriched components (Stracke et al., 2005), as shown by Hf and Nd isotopic data (Fig. 14).

All THO lavas seem to be derived from an Indian Ocean depleted MORB source mantle (I-DMM), similar to the source of the Oman ophiolitic gabbros. The addition of high field

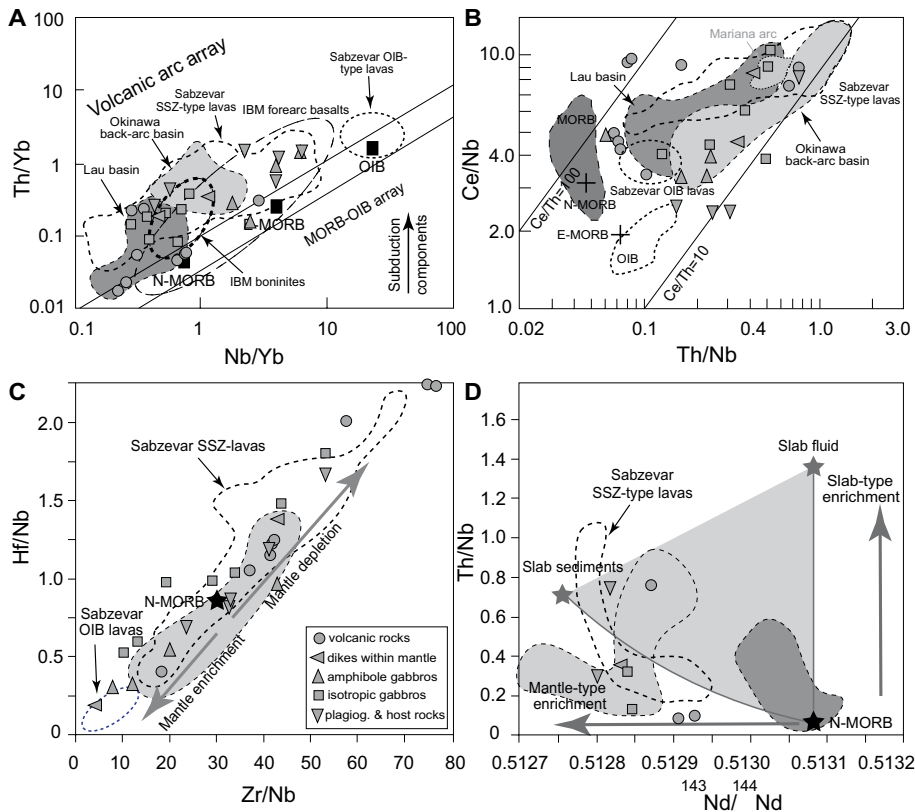


Figure 16. (A) Th/Yb vs. Ta/Yb (Pearce and Peate, 1995) and (B) Ce/Nb vs. Th/Nb (Sandeman et al., 2006) diagrams for the Torbat-e-Heydarieh magmatic rocks. Hf/Nb vs. Zr/Nb (C) and Th/Nb vs. $^{143}\text{Nd}/^{144}\text{Nd}$ plots (D) (Sorbadere et al., 2013) for Torbat-e-Heydarieh ophiolite magmatic rocks, Okinawa Trough, Central Lau basin and Sabzevar ophiolitic igneous rocks, comparing the effect of enrichment and depletion in the mantle sources of these magmas, with respect to the normal mid-ocean-ridge basalt (N-MORB) source. The gray field between slab fluid, slab sediments and N-MORB show bulk mixing between N-MORB and fluid and thus represents the slab contribution (modified after Sorbadere et al., 2013). Data from the Sabzevar ophiolite are from Moghadam et al. (2014a). Data from the Lau back-arc basin and the Okinawa Trough are from Tian et al. (2011) and Shinjo (1999) respectively. SSZ—supra-subduction zone.

strength elements such as Hf occurs if subducted sediments are melted or if supercritical fluids are involved (Kessel et al., 2005). The THO igneous rocks vary modestly in ϵHf and ϵNd , indicating restricted contributions of subducted sediment melts. We conclude that the THO pillow lavas and massive lavas reflect derivation from an Indian Ocean depleted MORB mantle that may have been slightly affected by melts of subducted sediments, although some isotropic gabbros and E-MORB lavas show a modestly-enriched mantle signature.

It is worth noting that THO Hf-isotope compositions are similar to those of the Zagros fore-arc ophiolites, both inner belt (Nain-Baft; $\epsilon\text{Hf}(t) = +8 - +21$) and outer belt (Neyriz-Kermanshah; $\epsilon\text{Hf}(t) = +10 - +23$) ophiolites, confirming a broadly similar mantle source for the generation of Late Cretaceous Iranian ophiolitic

magmas. However, the conspicuous variations in the zircon ϵHf values (+8.1 – +18.5) (which are similar to the whole-rock Hf isotope variations; $\epsilon\text{Hf} = +14.9 - +21.5$), can reflect mixing with new pulses of similar magmas but with slight isotopic differences entering the magma chamber during cooling of the plagiogranitic melts (Shaw and Flood, 2009).

Heterogeneous Mantle Sources for Torbat-e-Heydarieh Ophiolite Magmas: Further Thoughts

Table 1 summarizes possible sources and tectonic affinities of the studied THO rocks. As discussed above, lherzolites and impregnated lherzolites are similar to MOR abyssal peridotite. Dunites are most like SSZ-FA mantle whereas plagioclase lherzolites are most like sub-arc mantle. Plagiogranites and amphibole gabbros

also have strong arc affinities. Lavas, dikes in peridotite, other gabbros, and harzburgites have the strongest affinities with BAB (Table 1).

Cumulate gabbros are melt-deficient equivalents of isotropic gabbros; both are probably derived from Nb-Ta depleted N-MORB-like magmas like THO pillow and sheet lavas. Harzburgite is probably melt-depleted residual BAB mantle as indicated by Cr# and TiO_2 contents of its spinels (Fig. 10). The Cpx-harzburgite is similar to melt-impregnated harzburgite but with greater addition of abyssal basalt melt (Fig. 10A). “Abyssal basalt” in this case is not N-MORB but BAB basalt with signatures of slab-derived fluids. Cpx-harzburgites may represent reactive melt flow channels (Kimura and Sano, 2012). Magmas so generated could have formed dikes within the mantle near the Moho mantle and could have fractionated to form isotropic and cumulate gabbros. Some of this magma may have erupted as pillow lavas and sheet lavas to form BAB oceanic crust Layer 2 (Hirahara et al., 2015).

The presence of heterogeneous mantle rocks (with affinities to FA, IA, and MOR) associated with THO BAB is consistent with the inferred tectonic setting of the THO.

Tectonic Significance of the Torbat-e-Heydarieh Ophiolite

Timing of Back-arc Basin Opening and Its Relation to Zagros Subduction Initiation

Strong upper plate extension accompanies the initiation of some subduction zones such the Izu-Bonin-Mariana convergent margin, south of Japan. Strong extension on the upper plate of a nascent subduction zone, above the sinking lithosphere, allows asthenospheric upwelling and leads to seafloor spreading, forming infant arc crust of the proto-fore-arc (Stern, 2004; Stern and Gerya, 2017). Gurnis et al. (2004) and Hall et al. (2003) suggest that rapid trench retreat and extension in the overriding plate also occur after subduction becomes self-sustaining; others believe that trench roll-back (and back-arc extension) can start after the slab pull becomes greater than the far-field push (Baes et al., 2011).

Late Cretaceous Zagros ophiolites and their ~3000-km-long equivalents in Oman and from the Mediterranean area (Cyprus, Turkey, Syria to Iraq) show a site of Late Cretaceous subduction initiation along the southern margin of Eurasia (Moghadam and Stern, 2011; Monsef et al., 2018). The chemo-stratigraphic relationships of the lavas from these ophiolites, integrated with mantle geochemistry and paleomagnetic data, support the idea of arc infancy at the southern margin of Eurasia during the Late Cretaceous (Dilek et al., 2007; Maffione et al.,

2017; Moghadam and Stern, 2011; Monsef et al., 2018; Pearce and Robinson, 2010). It is also suggested that the earliest subduction stage after the SI coincided with the transient transfer of high-pressure rocks from the top of the subducting slab to the overriding plate (van Hinsbergen et al., 2015). Late Cretaceous high-pressure rocks are common within the Oman and Zagros ophiolites (Guilmette et al., 2018; Moghadam et al., 2017a), and further attest to the transfer of deep-seated rocks during the earliest stage of subduction.

Because of their setting far to the north of the Late Cretaceous Zagros SI plate margin, STHO ophiolites must have formed in a back-arc basin. They are easily related to the Late Cretaceous (ca. 104–98 Ma) formation of a new subduction zone along the southern margin of Iran, where seafloor spreading formed new oceanic lithosphere (Zagros inner and outer belts ophiolites) (Moghadam and Stern, 2015). Subduction initiation was followed quickly by arc magmatism to form the Urumieh-Dokhtar Magmatic Belt (e.g., Chiu et al., 2013; Ghasemi and Manesh, 2015; Ghorbani et al., 2014; Honarmand et al., 2014). Opening of the STHO BAB probably reflected strong regional extension of the overriding plate during subduction initiation. Our zircon U-Pb ages range from ca. 99 to 92 Ma, reflecting a period of ~7 m.y. for formation of the THO ophiolite. A similar age range is also indicated by Cenomanian to Turonian (ca. 99–90 Ma) carbonates deposited over the massive and pillow lavas.

Such a broad zone of extension accompanying SI is consistent with IODP 351 drilling results west of the Izu-Bonin-Mariana arc, where scientists were surprised to find Eocene basalts far west of where subduction began at ca. 51 Ma (Hickey-Vargas et al., 2018). The dominance of Late Cretaceous extension in NE Iran is also confirmed by the presence of a sheeted dike complex in the Sabzevar ophiolites with U-Pb ages of ca. 90 Ma obtained from the felsic dikes (Moghadam et al., 2014b). This extension was also associated with basement-involved low-angle normal faulting, core complex exhumation, block tilting, and sedimentary basin formation in some parts of Iran (e.g., in Saghand, Fig. 1 [Verdel et al., 2007], in Golpayegan [Moritz and Ghazban, 1996], and in Torud [Malekpour-Alamdari et al., 2017]), attested by ^{39}Ar - ^{40}Ar and K-Ar ages. These results show that extensional deformation prevailed during Late Cretaceous in what is now the Iranian plateau. Extension in NE Iran also generated a volcano-sedimentary basin (southern Sabzevar basin, N-NW of Oryan), which was filled by Late Cretaceous pelagic sediments, green siliceous tuffs, and submarine volcanic rocks (Kazemi et al., 2019). Late Cre-

taceous extension also allowed asthenospheric melts with radiogenic isotopic compositions to invade the continental crust and generate granitoids and lavas with radiogenic Nd and zircon Hf isotopic compositions (e.g., Alaminia et al., 2013; Kazemi et al., 2019).

Tectonic Setting of the Torbat-e-Heydarieh Ophiolite

Three key questions concerning the THO are addressed here. (1) What is the relationship between the Sabzevar and Torbat-e-Heydarieh ophiolites? (2) What is the relationship between STHO ophiolites and other ophiolites of similar age in eastern Iran? (3) What is the relationship between the Zagros fore-arc ophiolites and the STHO?

The ages obtained here agree with U-Pb zircon ages of 100–78 Ma for the Sabzevar ophiolite (Moghadam et al., 2014a). THO ages are also similar to zircon U-Pb ages obtained for dacitic-andesitic lavas from the Cheshmeshir and Oryan ophiolites (ca. 102–76 Ma, Fig. 3; Kazemi et al., 2019). Some of the younger ages may reflect arc magmatism. Together, results from the Torbat-e-Heydarieh, Sabzevar, and Cheshmehshir-Oryan ophiolites indicate a Late Cretaceous oceanic basin that was magmatically active and perhaps open for ~26 m.y. Our age results indicate that the Zagros SI may be somewhat older than the formation of the NE Iran back-arc basins (104–98 Ma versus 99–92 Ma).

Late Cretaceous mantle upwelling accompanying extension led to the emplacement of several juvenile intrusions and associated extrusive rocks (Late Cretaceous–Eocene magmatic belt in Fig. 3). These Late Cretaceous igneous rocks are abundant in NE Iran and are mostly juvenile additions from the mantle to the crust. Xenocrystic zircons (with ages of 1.1–1.5 Ga) from sample TH11-29 (diabasic dike within peridotites) suggest that recycling of ancient subducted materials accompanied back-arc opening. These xenocrystic zircons are found in many Neotethyan ophiolites in China and the Mediterranean realm (e.g., Gong et al., 2016; Robinson et al., 2015).

The THO probably represents an extension of the Sabzevar ophiolite. Although the formation age of these ophiolites (Sabzevar and THO) is nearly synchronous, there are striking differences in the tectono-metamorphic evolution of the two ophiolite belts. The main differences include the following. (1) Mantle peridotites are more important in the THO and spinels from Sabzevar mantle peridotites have SSZ-type or fore-arc-type signatures, characterized by higher Cr# (Shafaii Moghadam et al., 2015) (Fig. 10B). (2) Podiform chromitites are rare in the THO and abundant in the Sabzevar ophiolite. (3) Acidic volcanic rocks are abundant in Sabzevar,

whereas mafic volcanics are more important in the THO (Fig. 13A). Sabzevar volcanic rocks show more pronounced arc signatures than do those of the THO, indicated by higher Th/Yb, Th/Nb, and Ce/Nb ratios (Figs. 15A, 15B). (4) OIB-type lavas are present in Sabzevar (Moghadam et al., 2014a) but are absent in the THO, although the latter contains minor E-MORB. (5) The Sabzevar ophiolite marks an orogenic suture, with a Paleocene high-pressure/low-temperature metamorphic core (Omrani et al., 2013; Rossetti et al., 2014) and an external thrust-and-fold belt, showing evidence of a ductile-to-brittle top-to-the-SSE sense of tectonic transport (Rossetti et al., 2014). Moreover, a HP granulite event, Albian in age, may exist in the Sabzevar zone (Nasrabad et al., 2011; Rossetti et al., 2010). Conversely, the THO realm does not show evidence of orogenic metamorphism, and the post-Cretaceous tectonic evolution has been controlled by polyphase strike-slip shearing (Tadayon et al., 2017).

The observation that all Sabzevar lavas and mantle peridotites have SSZ signatures whereas THO lavas and peridotites have mostly MORB-like signatures, as well as the presence of older high-P rocks in the Sabzevar and their absence in the Torbat-e-Heydarieh, may indicate that the Torbat-e-Heydarieh and Sabzevar ophiolites represent distinct back-arc basins, differing proximities to the arc, or different stages in BAB opening. It is probably not realistic to consider two neighboring oceanic basins so close together in NE Iran during Late Cretaceous time, although distinct rift basins existed due to strike-slip faulting accompanying break-up of the continental lithosphere in NE Iran. We prefer to interpret STHO ophiolite fragments as having formed in a single back-arc basin, perhaps in distinct extensional basins (grabens), developed during Late Cretaceous hyperextension in the region.

Regarding the second question, what is the relationship of STHO to other Late Cretaceous oceanic remnants in eastern Iran? We believe that back-arc opening experienced distinct spatio-temporal and geodynamic evolution, but nearly all formed due to the extensional regime which prevailed in the region during the latest Early to Late Cretaceous (ca. 110–70 Ma). The Birjand-Zahedan ophiolites in eastern Iran (Fig. 1) are similar in age to the STHO. SHRIMP U-Pb zircon dating of metafelsic rocks and eclogites from the Birjand-Zahedan ophiolites gave ages of ca. 86–89 Ma (Bröcker et al., 2013) (Fig. 13). In addition, zircon U-Pb ages from Birjand-Zahedan gabbros are somewhat older than STHO ophiolites, 113–107 Ma (Zarinkoub et al., 2012). These may be related to a different episode of Early Cretaceous subduction in the region. Zircon and titanite from felsic

TABLE 1. PROVENANCE OF THE MANTLE-CRUST-LAVA UNITS OF TORBAT-E-HEYDARIEH OPHIOLITE

Rock/provenance	Mid-ocean-ridge	SSZ-FA	SSZ-IA	Back-arc basin
Lava				Lava (pillow/massive) Dikes within mantle
Crust			Plagiogranite amphibole gabbro	
Mantle	Lherzolite Impregnated lherzolite	Dunite	Plagioclase lherzolite	Isotropic gabbro Cumulate gabbro Harzburgite Cpx-harzburgite

Note: SSZ-FA—supra-subduction zone—fore-arc; SSZ-IA—supra-subduction zone— island arc; Cpx—clinopyroxene.

segregations in mafic granulites from the Sabzevar ophiolite yield U-Pb ages of 107.4 ± 2.4 and 105.9 ± 2.3 Ma, respectively (Fig. 13; Rossetti et al., 2010). This evidence might suggest the formation of Early Cretaceous (i.e., pre-Albian) Sabzevar-Birjand-Zahedan single oceanic realm in the upper plate above a Neotethys subduction zone. In fact, the formation of these high-P granulites in a subduction zone is questionable, as these rocks contain no high-P minerals, their zircon U-Pb age (ca. 107 Ma) is similar to their titanite age (ca. 105 Ma), and both are similar to the zircon U-Pb ages reported from the felsic to mafic magmatic rocks from the Sabzevar area (Fig. 3). Therefore, we believe these metamorphic rocks (with amphibole-plagioclase-garnet \pm titanite as rock-forming minerals) had a mafic protolith and were not metamorphosed in a subduction zone. It seems that a MORB precursor related to 105 Ma granulites existed in the Sabzevar area during the Lower Cretaceous (Nasrabad et al., 2011). This may imply that an oceanic crust older than 105 Ma was present in NE Iran, before the Torbat-e- Heydariéh back-arc basin started to open.

Finally, what is the relationship between Zagros ophiolites and the STHO? There are geochemical similarities, but Zagros ophiolites are mostly slightly older (ca. 104–98 Ma) than the STHO (ca. 99–80 Ma). This may reflect the migration of extension accompanying subduction initiation; first in what becomes the fore-arc, then as the slab descends the locus of extension migrates to the back-arc region (Fig. 17A). In this scenario, the STHO represents a back-arc basin that formed behind the Zagros fore-arc and the nascent Urumieh-Dokhtar magmatic arc (Fig. 17B). Back-arc opening would have disrupted Cadomian continental crust, including Cadomian subcontinental lithospheric mantle (SCLM; the Lu-Hf versus Hf plot, not shown, indicates an isochron with a Cadomian mantle-depletion age of ca. 585 Ma). Involvement of such subcontinental lithospheric mantle may explain the origin of OIB-type lavas in the Sabzevar ophiolite and E-MORB in THO. How far west this back-arc basin can be traced remains unclear, because

the region to the SW between the STHO and the Nain ophiolites of similar age is covered by younger deposits for ~ 400 km (Fig. 1). Geophysical studies of this region including magnetics and gravity may help answer this question.

The question of when and why the STHO BAB collapsed is also unresolved. U-Pb ages for THO indicate a lifespan of ~ 7 m.y., slightly less than the lifespan of 12.5 ± 4.7 m.y. for global extinct BABs (Stern and Dickinson, 2010). One possibility is that the Iranian continental lithosphere had been weakened by prolonged arc igneous activity, allowing the basin to collapse

when regional stress changed from extension to compression as the subduction zone evolved. There is abundant evidence for prolonged arc igneous activity from Late Cretaceous time onward (e.g., Chiu et al., 2013; Honarmand et al., 2014; Hosseini et al., 2017; Verdel et al., 2011). The volcano-pelagic series above the STHO includes Cenomanian to Maastrichtian deep-sea pelagic sediments interbedded with pyroclastic and andesitic to dacitic lavas. Dacitic-andesitic lavas from the Cheshmehshir and Oryan ophiolites have Late Cretaceous (ca. 102–76 Ma) U-Pb ages (Kazemi et al., 2019). This sequence grades upward into a series of Maastrichtian to Paleocene shallow water sediments and then into the Oryan marine sediments (lower and middle Oryan sediments) from early Eocene to early middle Eocene. Moreover, zircon U-Pb ages for plutonic rocks from south of Sabzevar and Neyshabour (Fig. 3, between the Sabzevar ophiolite in the north and the Cheshmehshir ophiolite in the south) are of Cenomanian-Maastrichtian (97.0 ± 0.2 Ma; 67.5 ± 0.5 Ma) to Oligo-Miocene (29.8 ± 0.2 Ma) (Moghadam et al., unpublished data; Alaminia et al., 2013). The Late Cretaceous ages are similar to the

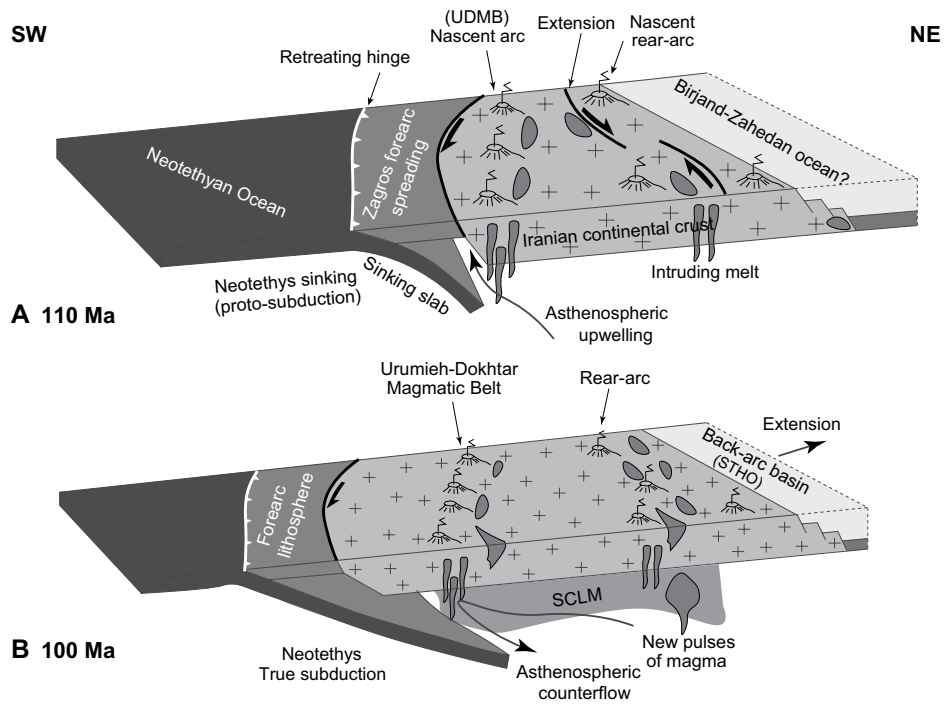


Figure 17. Schematic model showing the generation of the Sabzevar-Torbat-e-Heydariéh ophiolites. (A) Subduction initiation and Neotethys sinking caused strong extension in the region above the sinking lithosphere, leading to seafloor spreading and forming the proto-fore-arc crust. Strong extension in the Iranian continental crust lead to extensional basins opening and nucleation of the Sabzevar-Torbat-e-Heydariéh ophiolites (STHO) back-arc basin. UDM—Urumieh-Dokhtar Magmatic Belt. (B) Beginning of true subduction (ca. 100 Ma), and formation of the Urumieh-Dokhtar arc and the STHO back-arc basin. SCLM—subcontinental lithospheric mantle.

U-Pb zircon ages of the Sabzevar plagiogranites (100–78 Ma).

CONCLUSIONS

Our study of the THO confirms that it formed in Late Cretaceous time. Dikes intruding THO mantle peridotites and plagiogranites have U-Pb ages of 99–92 Ma. THO igneous rocks have a range of $\epsilon\text{Nd}(t)$ between +5.7 and +8.2 and their $\epsilon\text{Hf}(t)$ values range from +14.9 to +21.5; THO zircons have $\epsilon\text{Hf}(t)$ values of +8.1 to +18.5. Like all NE Iran ophiolites, the THO is found in a tectonic position well to the north of slightly older Zagros fore-arc ophiolites and the Urumieh-Dokhtar magmatic belt, and thus appears to have formed as a continental back-arc basin. Petrological, geochemical, and isotopic compositions are consistent with this interpretation. THO peridotites contain spinels and clinopyroxenes with compositions like those in peridotites from mid-ocean ridges and back-arc basins. THO igneous rocks have Hf-Nd isotopic compositions that are similar to Indian Ocean MORBs and do not show clear evidence for addition of sediment-derived melts or fluids from a subducted slab. Magmatic rocks in the THO show both MORB-like and SSZ geochemical signatures. We conclude that formation of the Sabzevar–Torbat-e-Heydarieh ophiolite reflects opening of a Late Cretaceous back-arc basin as a result of regional hyper-extension accompanying subduction initiation along southern Iran.

ACKNOWLEDGMENTS

This is contribution 1236 from the ARC Centre of Excellence for Core to Crust Fluid Systems (<http://www.ccfcs.mq.edu.au>), 1275 from the GEMOC Key Centre (<http://www.gemoc.mq.edu.au>), and UTD Geosciences contribution number 1343, and is related to IGCP-662. Zircon U-Pb geochronology, clinopyroxene in situ trace elements, and zircon Lu-Hf isotope data were obtained using instrumentation funded by DEST Systemic Infrastructure Grants, ARC LIEF, NCRIS/AuScope, industry partners, and Macquarie University. We thank Prof S. Arai for his support during electron microprobe analysis at Kanazawa University. We are very grateful to Federico Rossetti, an anonymous reviewer, and *GSA Bulletin's* associate editor for their constructive reviews of the manuscript. Editorial suggestions by Brad Singer are appreciated. All logistical support for field studies came from Damghan University.

REFERENCES CITED

Agard, P., Jolivet, L., Vrielynck, B., Burov, E., and Monie, P., 2007, Plate acceleration: The obduction trigger?: *Earth and Planetary Science Letters*, v. 258, no. 3–4, p. 428–441, <https://doi.org/10.1016/j.epsl.2007.04.002>.
 Alaminia, Z., Karimpour, M.H., Homam, S.M., and Finger, F., 2013, The magmatic record in the Arghash region (northeast Iran) and tectonic implications: *International Journal of Earth Sciences*, v. 102, no. 6, p. 1603–1625, <https://doi.org/10.1007/s00531-013-0897-1>.
 Aldanmaz, E., 2012, Trace element geochemistry of primary mantle minerals in spinel-peridotites from polygenetic

MOR-SSZ suites of SW Turkey: constraints from an LA-ICP-MS study and implications for mantle metasomatism: *Geological Journal*, v. 47, no. 1, p. 59–76, <https://doi.org/10.1002/gj.1336>.
 Anenburg, M., Katzir, Y., Rhede, D., Jons, N., and Bach, W., 2015, Rare earth element evolution and migration in plagiogranites: a record preserved in epidote and allanite of the Troodos ophiolite: *Contributions to Mineralogy and Petrology*, v. 169, no. 3, <https://doi.org/10.1007/s00410-015-1114-y>.
 Arai, S., Kadoshima, K., and Morishita, T., 2006, Widespread arc-related melting in the mantle section of the northern Oman ophiolite as inferred from detrital chromian spinels: *Journal of the Geological Society*, v. 163, p. 869–879, <https://doi.org/10.1144/0016-76492005-057>.
 Baes, M., Govers, R., and Wortel, R., 2011, Subduction initiation along the inherited weakness zone at the edge of a slab: Insights from numerical models: *Geophysical Journal International*, v. 184, no. 3, p. 991–1008, <https://doi.org/10.1111/j.1365-246X.2010.04896.x>.
 Bağcı, U., Parlak, O., and Hock, V., 2005, Whole-rock and mineral chemistry of cumulates from the Kizildag (Hatay) ophiolite (Turkey): clues for multiple magma generation during crustal accretion in the southern Neotethyan ocean: *Mineralogical Magazine*, v. 69, no. 1, p. 53–76, <https://doi.org/10.1180/0026461056910234>.
 Bazylev, B.A., Popevic, A., Karamata, S., Kononkova, N.N., Simakin, S.G., Olujic, J., Vujnovic, L., and Memovic, E., 2009, Mantle peridotites from the Dinaridic ophiolite belt and the Vardar zone western belt, central Balkan: A petrological comparison: *Lithos*, v. 108, no. 1–4, p. 37–71, <https://doi.org/10.1016/j.lithos.2008.09.011>.
 Bédard, E., Hebert, R., Guilmette, C., Lesage, G., Wang, C.S., and Dostal, J., 2009, Petrology and geochemistry of the Saga and Sangsang ophiolitic massifs, Yarlung Zangbo Suture Zone, Southern Tibet: Evidence for an arc-back-arc origin: *Lithos*, v. 113, no. 1–2, p. 48–67, <https://doi.org/10.1016/j.lithos.2009.01.011>.
 Bizimis, M., Salters, V.J., and Bonatti, E., 2000, Trace and REE content of clinopyroxenes from supra-subduction zone peridotites. Implications for melting and enrichment processes in island arcs: *Chemical Geology*, v. 165, no. 1–2, p. 67–85, [https://doi.org/10.1016/S0009-2541\(99\)00164-3](https://doi.org/10.1016/S0009-2541(99)00164-3).
 Bonev, N., and Stampfli, G., 2009, Gabbro, plagiogranite and associated dykes in the supra-subduction zone Evros Ophiolites, NE Greece: *Geological Magazine*, v. 146, no. 1, p. 72–91, <https://doi.org/10.1017/S0016756808005396>.
 Bröcker, M., Fotoohi Rad, G.F., Burgess, R., Theunissen, S., Paderin, I., Rodionov, N., and Salimi, Z., 2013, New age constraints for the geodynamic evolution of the Sistan Suture Zone, eastern Iran: *Lithos*, v. 170, p. 17–34, <https://doi.org/10.1016/j.lithos.2013.02.012>.
 Burns, L.E., 1985, The Border Ranges ultramafic and mafic complex, south-central Alaska—Cumulate fractionates of island-arc volcanics: *Canadian Journal of Earth Sciences*, v. 22, no. 7, p. 1020–1038, <https://doi.org/10.1139/e85-106>.
 Burtman, V., 1994, Meso-Tethyan oceanic sutures and their deformation: *Tectonophysics*, v. 234, no. 4, p. 305–327, [https://doi.org/10.1016/0040-1951\(94\)90230-5](https://doi.org/10.1016/0040-1951(94)90230-5).
 Cawood, P.A., 1989, Acadian remobilization of a Taconian ophiolite, Hare Bay Allochthon, northwestern Newfoundland: *Geology*, v. 17, no. 3, p. 257–260, [https://doi.org/10.1130/0091-7613\(1989\)017<257:AROA TO>2.3.CO;2](https://doi.org/10.1130/0091-7613(1989)017<257:AROA TO>2.3.CO;2).
 Chauvel, C., and Blichert-Toft, J., 2001a, A hafnium isotope and trace element perspective on melting of the depleted mantle: *Earth and Planetary Science Letters*, v. 190, no. 3, p. 137–151, [https://doi.org/10.1016/S0012-821X\(01\)00379-X](https://doi.org/10.1016/S0012-821X(01)00379-X).
 Chauvel, C., and Blichert-Toft, J., 2001b, A hafnium isotope and trace element perspective on melting of the depleted mantle: *Earth and Planetary Science Letters*, v. 190, no. 3–4, p. 137–151, [https://doi.org/10.1016/S0012-821X\(01\)00379-X](https://doi.org/10.1016/S0012-821X(01)00379-X).
 Chauvel, C., Marini, J.C., Plank, T., and Ludden, J.N., 2009, Hf-Nd input flux in the Izu-Mariana subduction zone and recycling of subducted material in the mantle: *Geochimistry Geophysics Geosystems*, v. 10, no. 1, <https://doi.org/10.1029/2008GC002101>.

Chiu, H.Y., Chung, S.L., Zarrinkoub, M.H., Mohammadi, S.S., Khatib, M.M., and Izuka, Y., 2013, Zircon U-Pb age constraints from Iran on the magmatic evolution related to Neotethyan subduction and Zagros orogeny: *Lithos*, v. 162, p. 70–87, <https://doi.org/10.1016/j.lithos.2013.01.006>.
 Coleman, R.G., 1977, *Ophiolites*: New York, Springer-Verlag, 220 p.
 Dercourt, J., Zonenshain, L.P., Ricou, L.E., Kazmin, V.G., Lepichon, X., Knipper, A.L., Grandjacquet, C., Sbertshikov, I.M., Geysant, J., Lepvrier, C., Pecharsky, D.H., Boulin, J., Sibuet, J.C., Savostin, L.A., Sorokhtin, O., Westphal, M., Bazhenov, M.L., Lauer, J.P., and Bijuval, B., 1986, Geological evolution of the Tethys Belt from the Atlantic to the Pamirs since the Lias: *Tectonophysics*, v. 123, no. 1–4, p. 241–315, [https://doi.org/10.1016/0040-1951\(86\)90199-X](https://doi.org/10.1016/0040-1951(86)90199-X).
 Dick, H.J.B., and Bullen, T., 1984, Chromian spinel as a petrogenetic indicator in abyssal and Alpine-type peridotites and spatially associated lavas: *Contributions to Mineralogy and Petrology*, v. 86, no. 1, p. 54–76, <https://doi.org/10.1007/BF00373711>.
 Dilek, Y., and Flower, M.F.J., 2003, Arc-trench rollback and forearc accretion: 2. A model template for ophiolites in Albania, Cyprus, and Oman: *Ophiolites in Earth History*, v. 218, p. 43–68.
 Dilek, Y., and Furnes, H., 2009, Structure and geochemistry of Tethyan ophiolites and their petrogenesis in subduction rollback systems: *Lithos*, v. 113, no. 1–2, p. 1–20, <https://doi.org/10.1016/j.lithos.2009.04.022>.
 Dilek, Y., and Furnes, H., 2011, Ophiolite genesis and global tectonics: Geochemical and tectonic fingerprinting of ancient oceanic lithosphere: *Geological Society of America Bulletin*, v. 123, no. 3–4, p. 387–411, <https://doi.org/10.1130/B30446.1>.
 Dilek, Y., and Thy, P., 2006, Age and petrogenesis of plagiogranite intrusions in the Ankara melange, central Turkey: *The Island Arc*, v. 15, no. 1, p. 44–57, <https://doi.org/10.1111/j.1440-1738.2006.00522.x>.
 Dilek, Y., Furnes, H., and Shallo, M., 2007, Suprasubduction zone ophiolite formation along the periphery of Mesozoic Gondwana: *Gondwana Research*, v. 11, no. 4, p. 453–475, <https://doi.org/10.1016/j.gr.2007.01.005>.
 Furnes, H., de Wit, M., and Dilek, Y., 2014, Four billion years of ophiolites reveal secular trends in oceanic crust formation: *Geoscience Frontiers*, v. 5, no. 4, p. 571–603, <https://doi.org/10.1016/j.gsf.2014.02.002>.
 Gerya, T., 2011, Intra-oceanic Subduction Zones, in Brown, D., and Ryan, P.D., eds., *Arc-Continent Collision*, *Frontiers in Earth Sciences*: Berlin, Springer-Verlag, p. 23–53, https://doi.org/10.1007/978-3-540-88558-0_2.
 Ghasemi, A., and Manesh, S.M.T., 2015, Geochemistry and petrogenesis of Gohroud Igneous Complex (Urumieh-Dokhtar zone): evidence for Neotethyan subduction during the Neogene: *Arabian Journal of Geosciences*, v. 8, no. 11, p. 9599–9623, <https://doi.org/10.1007/s12517-015-1883-7>.
 Ghazi, A., Hassanipak, A., and Wallace, K., 1997, Geochemistry, petrology and geology of the Sabzevar ophiolite, Northeastern Iran: Implication on Tethyan tectonics: *Geological Society of America Abstracts with Programs*, v. 29, p. A-229.
 Ghazi, J.M., Moazzen, M., Rahgoshay, M., and Moghadam, H.S., 2010, Mineral chemical composition and geodynamic significance of peridotites from Nain ophiolite, central Iran: *Journal of Geodynamics*, v. 49, no. 5, p. 261–270, <https://doi.org/10.1016/j.jog.2010.01.004>.
 Ghorbani, M.R., Graham, I.T., and Ghaderi, M., 2014, Oligocene-Miocene geodynamic evolution of the central part of Urumieh-Dokhtar Arc of Iran: *International Geology Review*, v. 56, no. 8, p. 1039–1050, <https://doi.org/10.1080/00206814.2014.919615>.
 Gong, X.H., Shi, R.D., Griffin, W.L., Huang, Q.S., Xiong, Q., Chen, S.S., Zhang, M., and O'Reilly, S.Y., 2016, Recycling of ancient subduction-modified mantle domains in the Purang ophiolite (southwestern Tibet): *Lithos*, v. 262, p. 11–26, <https://doi.org/10.1016/j.lithos.2016.06.025>.
 Guilmette, C., Smit, M.A., van Hinsbergen, D.J.J., Gürer, D., Corfu, F., Charette, B., Maffione, M., Rabeau, O., and Savard, D., 2018, Forced subduction initiation recorded in the sole and crust of the Semail Ophiolite

- Oman: *Nature Geoscience*, v. 11, p. 688–695, <https://doi.org/10.1038/s41561-018-0209-2>.
- Gurnis, M., Hall, C., and Lavier, L., 2004, Evolving force balance during incipient subduction: *Geochemistry Geophysics Geosystems*, v. 5, <https://doi.org/10.1029/2003GC000681>.
- Haase, K.M., Freund, S., Koepke, J., Hauff, F., and Erdmann, M., 2015, Melts of sediments in the mantle wedge of the Oman ophiolite: *Geology*, v. 43, no. 4, p. 275–278, <https://doi.org/10.1130/G36451.1>.
- Hall, C.E., Gurnis, M., Scrolias, M., Lavier, L.L., and Muller, R.D., 2003, Catastrophic initiation of subduction following forced convergence across fracture zones: *Earth and Planetary Science Letters*, v. 212, no. 1–2, p. 15–30, [https://doi.org/10.1016/S0012-821X\(03\)00242-5](https://doi.org/10.1016/S0012-821X(03)00242-5).
- Hamada, M., and Fujii, T., 2008, Experimental constraints on the effects of pressure and H₂O on the fractional crystallization of high-Mg island arc basalt: Contributions to Mineralogy and Petrology, v. 155, no. 6, p. 767–790, <https://doi.org/10.1007/s00410-007-0269-6>.
- Hébert, R., Bezard, R., Guilmette, C., Dostal, J., Wang, C.S., and Liu, Z.F., 2012, The Indus–Yarlung Zangbo ophiolites from Nanga Parbat to Namche Barwa syntaxes, southern Tibet: First synthesis of petrology, geochemistry, and geochronology with incidences on geodynamic reconstructions of Neo-Tethys: *Gondwana Research*, v. 22, no. 2, p. 377–397, <https://doi.org/10.1016/j.gr.2011.10.013>.
- Hickey-Vargas, R., Yogodzinski, G., Ishizuka, O., McCarthy, A., Bizimis, M., Kusano, Y., Savov, I., and Arculus, R., 2018, Origin of depleted basalts during subduction initiation and early development of the Izu-Bonin-Mariana Island arc: Evidence from IODP Expedition 351 Site U1438, Amami-Sankaku Basin: *Geochimica et Cosmochimica Acta*, v. 229, p. 85–111, <https://doi.org/10.1016/j.gca.2018.03.007>.
- Hirahara, Y., Kimura, J.I., Senda, R., Miyazaki, T., Kawabata, H., Takahashi, T., Chang, Q., Vaglarov, B.S., Sato, T., and Kodaira, S., 2015, Geochemical variations in Japan Sea back-arc basin basalts formed by high-temperature adiabatic melting of mantle metasomatized by sediment subduction components: *Geochemistry Geophysics Geosystems*, v. 16, no. 5, p. 1324–1347, <https://doi.org/10.1002/2015GC005720>.
- Honarmand, M., Omran, N.R., Neubauer, F., Emami, M.H., Nabatian, G., Liu, X.M., Dong, Y.P., von Quadt, A., and Chen, B., 2014, Laser-ICP-MS U-Pb zircon ages and geochemical and Sr-Nd-Pb isotopic compositions of the Niyasar plutonic complex, Iran: constraints on petrogenesis and tectonic evolution: *International Geology Review*, v. 56, no. 1, p. 104–132, <https://doi.org/10.1080/00206814.2013.820375>.
- Hosseini, M.R., Hassanzadeh, J., Alirezaei, S., Sun, W.D., and Li, C.Y., 2017, Age revision of the Neotethyan arc migration into the southeast Urumieh-Dokhtar belt of Iran: *Geochemistry and U-Pb zircon geochronology: Lithos*, v. 284, p. 296–309, <https://doi.org/10.1016/j.lithos.2017.03.012>.
- Ishikawa, T., Nagaishi, K., and Umino, S., 2002, Boninitic volcanism in the Oman ophiolite: Implications for thermal condition during transition from spreading ridge to arc: *Geology*, v. 30, no. 10, p. 899–902, [https://doi.org/10.1130/0091-7613\(2002\)030<899:BVITOO>2.0.CO;2](https://doi.org/10.1130/0091-7613(2002)030<899:BVITOO>2.0.CO;2).
- Ishizuka, O., Tani, K., and Reagan, M.K., 2014, Izu-Bonin-Mariana forearc crust as a modern ophiolite analogue: *Elements*, v. 10, no. 2, p. 115–120, <https://doi.org/10.2113/gselements.10.2.115>.
- Johnson, K., Dick, H.J., and Shimizu, N., 1990, Melting in the oceanic upper mantle: an ion microprobe study of diopsides in abyssal peridotites: *Journal of Geophysical Research*, *Solid Earth*, v. 95, no. B3, p. 2661–2678, <https://doi.org/10.1029/JB095iB03p02661>.
- Kazemi, Z., Ghasemi, H., Tilhac, R., Griffin, W., Moghadam, H.S., O'Reilly, S., and Mousivand, F., 2019, Late Cretaceous subduction-related magmatism on the southern edge of Sabzevar basin, NE Iran: *Journal of the Geological Society*, v. 176, p. 530–552, <https://doi.org/10.1144/jgs2018-076>.
- Kazmin, V.G., Sborshikov, I.M., Ricou, L.E., Zonenshain, L.P., Boulin, J., and Knipper, A.L., 1986, Volcanic belts as markers of the Mesozoic-Cenozoic active margin of Eurasia: *Tectonophysics*, v. 123, no. 1–4, p. 123–152, [https://doi.org/10.1016/0040-1951\(86\)90195-2](https://doi.org/10.1016/0040-1951(86)90195-2).
- Kelley, K.A., Kingsley, R., and Schilling, J.G., 2013, Composition of plume-influenced mid-ocean ridge lavas and glasses from the Mid-Atlantic Ridge, East Pacific Rise, Galápagos Spreading Center, and Gulf of Aden: *Geochemistry Geophysics Geosystems*, v. 14, no. 1, p. 223–242, <https://doi.org/10.1002/ggge.20049>.
- Kessel, R., Schmidt, M.W., Ulmer, P., and Pettko, T., 2005, Trace element signature of subduction-zone fluids, melts and supercritical liquids at 120–180 km depth: *Nature*, v. 437, no. 7059, p. 724–727, <https://doi.org/10.1038/nature03971>.
- Khalatbari-Jafari, M., Juteau, T., Bellon, H., Whitechurch, H., Cotten, J., and Emami, H., 2004, New geological, geochronological and geochemical investigations on the Khoy ophiolites and related formations, NW Iran: *Journal of Asian Earth Sciences*, v. 23, no. 4, p. 507–535, <https://doi.org/10.1016/j.jseas.2003.07.005>.
- Khedr, M.Z., and Arai, S., 2009, Geochemistry of metasomatized peridotites above subducting slab: a case study of hydrous metaperidotites from Happono complex, central Japan: *Journal of Mineralogical and Petrological Sciences*, v. 104, no. 5, p. 313–318, <https://doi.org/10.2465/jmps.090611>.
- Kimura, J.-I., and Sano, S., 2012, Reactive melt flow as the origin of residual mantle lithologies and basalt chemistries in mid-ocean ridges: Implications from the Red Hills peridotite, New Zealand: *Journal of Petrology*, v. 53, no. 8, p. 1637–1671, <https://doi.org/10.1093/petrology/egs028>.
- Kimura, J.-I., Stern, R.J., and Yoshida, T., 2005, Reinitiation of subduction and magmatic responses in SW Japan during Neogene time: *Geological Society of America Bulletin*, v. 117, no. 7–8, p. 969–986, <https://doi.org/10.1130/B25565.1>.
- Lagabrielle, Y., Guivel, C., Maury, R.C., Bourgeois, J., Fourcade, S., and Martin, H., 2000, Magmatic-tectonic effects of high thermal regime at the site of active ridge subduction: the Chile Triple Junction model: *Tectonophysics*, v. 326, no. 3–4, p. 255–268, [https://doi.org/10.1016/S0040-1951\(00\)00124-4](https://doi.org/10.1016/S0040-1951(00)00124-4).
- Leake, B.E., Woolley, A.R., Arps, C.E.S., Birch, W.D., Gilbert, M.C., Grice, J.D., Hawthorne, F.C., Kato, A., Kisch, H.J., Krivovichev, V.G., Linthout, K., Laird, J., Mandarino, J., Maresch, W.V., Nickel, E.H., Rock, N.M.S., Schumacher, J.C., Smith, D.C., Stephenson, N.C.N., Ungaretti, L., Whittaker, E.J.W., and Youzhi, G., 1997, Nomenclature of amphiboles: Report of the Subcommittee on Amphiboles of the International Mineralogical Association Commission on New Minerals and Mineral Names: *Mineralogical Magazine*, v. 61, no. 2, p. 295–321.
- Long, M.D., and Wirth, E.A., 2013, Mantle flow in subduction systems: The mantle wedge flow field and implications for wedge processes: *Journal of Geophysical Research*, *Solid Earth*, v. 118, no. 2, p. 583–606, <https://doi.org/10.1002/jgrb.50063>.
- Maffione, M., van Hinsbergen, D.J.J., de Gelder, G.I.N.O., van der Goes, F.C., and Morris, A., 2017, Kinematics of Late Cretaceous subduction initiation in the Neo-Tethys Ocean reconstructed from ophiolites of Turkey, Cyprus, and Syria: *Journal of Geophysical Research*, *Solid Earth*, v. 122, no. 5, p. 3953–3976, <https://doi.org/10.1002/2016JB013821>.
- Maghfouri, S., Rastad, E., Mousivand, F., Lin, Y., and Zaw, K., 2016, Geology, ore facies and sulfur isotopes geochemistry of the Nuhed Besshi-type volcanogenic massive sulfide deposit, southwest Sabzevar basin, Iran: *Journal of Asian Earth Sciences*, v. 125, p. 1–21, <https://doi.org/10.1016/j.jseas.2016.04.022>.
- Malekpour-Alamdari, A., Axen, G., Heizler, M., and Hassanzadeh, J., 2017, Large-magnitude continental extension in the northeastern Iranian Plateau: Insight from K-feldspar ⁴⁰Ar/³⁹Ar thermochronology from the Shotor Kuh–Biarjand metamorphic core complex: *Geosphere*, v. 13, no. 4, p. 1207–1233, <https://doi.org/10.1130/GES01423.1>.
- McDonough, W.F., and Sun, S.S., 1995, The Composition of the Earth: *Chemical Geology*, v. 120, no. 3–4, p. 223–253, [https://doi.org/10.1016/0009-2541\(94\)00140-4](https://doi.org/10.1016/0009-2541(94)00140-4).
- Miyashiro, A., 1974, Volcanic rock series in island arcs and active continental margins: *American Journal of Science*, v. 274, no. 4, p. 321–355, <https://doi.org/10.2475/ajs.274.4.321>.
- Moghadam, H.S., and Stern, R.J., 2011, Geodynamic evolution of Upper Cretaceous Zagros ophiolites: formation of oceanic lithosphere above a nascent subduction zone: *Geological Magazine*, v. 148, no. 5–6, p. 762–801, <https://doi.org/10.1017/S0016756811000410>.
- Moghadam, H.S., and Stern, R.J., 2015, Ophiolites of Iran: Keys to understanding the tectonic evolution of SW Asia: (II) Mesozoic ophiolites: *Journal of Asian Earth Sciences*, v. 100, p. 31–59, <https://doi.org/10.1016/j.jseas.2014.12.016>.
- Moghadam, H.S., Stern, R.J., and Rahgoshay, M., 2010, The Dehshir ophiolite (central Iran): Geochemical constraints on the origin and evolution of the Inner Zagros ophiolite belt: *Geological Society of America Bulletin*, v. 122, no. 9–10, p. 1516–1547, <https://doi.org/10.1130/B30066.1>.
- Moghadam, H.S., Stern, R.J., Kimura, J.I., Hirahara, Y., Senda, R., and Miyazaki, T., 2012, Hf-Nd isotope constraints on the origin of Dehshir Ophiolite, Central Iran: The Island Arc, v. 21, no. 3, p. 202–214, <https://doi.org/10.1111/j.1440-1738.2012.00815.x>.
- Moghadam, H.S., Corfu, F., and Stern, R.J., 2013, U-Pb zircon ages of Late Cretaceous Nain-Dehshir ophiolites, central Iran: *Journal of the Geological Society*, v. 170, no. 1, p. 175–184, <https://doi.org/10.1144/jgs2012-066>.
- Moghadam, H.S., Corfu, F., Chiaradia, M., Stern, R.J., and Ghorbani, G., 2014a, Sabzevar Ophiolite, NE Iran: Progress from embryonic oceanic lithosphere into magmatic arc constrained by new isotopic and geochemical data: *Lithos*, <https://doi.org/10.1016/j.lithos.2014.10.004>.
- Moghadam, H.S., Corfu, F., Chiaradia, M., Stern, R.J., and Ghorbani, G., 2014b, Sabzevar Ophiolite, NE Iran: Progress from embryonic oceanic lithosphere into magmatic arc constrained by new isotopic and geochemical data: *Lithos*, v. 210, p. 224–241, <https://doi.org/10.1016/j.lithos.2014.10.004>.
- Moghadam, H.S., Khedr, M.Z., Arai, S., Stern, R.J., Ghorbani, G., Tamura, A., and Otley, C.J., 2015a, Arc-related harzburgite-dunite-chromitite complexes in the mantle section of the Sabzevar ophiolite, Iran: A model for formation of podiform chromitites: *Gondwana Research*, v. 27, no. 2, p. 575–593, <https://doi.org/10.1016/j.gr.2013.09.007>.
- Moghadam, H.S., Brocker, M., Griffin, W.L., Li, X.H., Chen, R.X., and O'Reilly, S.Y., 2017a, Subduction, high-P metamorphism, and collision fingerprints in South Iran: Constraints from zircon U-Pb and mica Rb-Sr geochronology: *Geochemistry Geophysics Geosystems*, v. 18, no. 1, p. 306–332, <https://doi.org/10.1002/2016GC006585>.
- Moghadam, H.S., Li, X.-H., Santos, J.F., Stern, R.J., Griffin, W.L., Ghorbani, G., and Sarebani, N., 2017b, Neoproterozoic magmatic flare-up along the N. margin of Gondwana: The Taknar complex, NE Iran: *Earth and Planetary Science Letters*, v. 474, p. 83–96, <https://doi.org/10.1016/j.epsl.2017.06.028>.
- Monsef, I., Rahgoshay, M., Mohajjel, M., and Moghadam, H.S., 2010, Peridotites from the Khoy Ophiolitic Complex, NW Iran: Evidence of mantle dynamics in a supra-subduction-zone context: *Journal of Asian Earth Sciences*, v. 38, no. 3–4, p. 105–120, <https://doi.org/10.1016/j.jseas.2009.10.007>.
- Monsef, I., Monsef, R., Mata, J., Zhang, Z., Pirouz, M., Rezaeian, M., Esmacili, R., and Xiao, W., 2018, Evidence for an early-MORB to fore-arc evolution within the Zagros suture zone: Constraints from zircon U-Pb geochronology and geochemistry of the Neyriz ophiolite (South Iran): *Gondwana Research*, <https://doi.org/10.1016/j.jgr.2018.03.002>.
- Moritz, R., and Ghazban, F., 1996, Geological and fluid inclusion studies in the Muteh gold district, Sanandaj-Sirjan zone, Isfahan Province, Iran: *Schweizerische Mineralogische und Petrographische Mitteilungen*, v. 76, no. 1, p. 85–89.
- Moritz, R., Ghazban, F., and Singer, B.S., 2006, Eocene gold ore formation at Muteh, Sanandaj-Sirjan tectonic zone, western Iran: A result of late-stage extension and exhumation of metamorphic basement rocks within the Zagros orogen: *Economic Geology and the Bulletin of the*

- Society of Economic Geologists, v. 101, no. 8, p. 1497–1524, <https://doi.org/10.2113/gsecongeo.101.8.1497>.
- Nasrabad, M., Rossetti, F., Theye, T., and Vignaroli, G., 2011, Metamorphic history and geodynamic significance of the Early Cretaceous Sabzevar granulites (Sabzevar structural zone, NE Iran): *Solid Earth*, v. 2, no. 2, p. 219–243, <https://doi.org/10.5194/se-2-219-2011>.
- Nicolas, A., 1989, *Structure of Ophiolites and Dynamics of Oceanic Lithosphere*: Dordrecht, The Netherlands, Kluwer Academic Publishers, 367 p.
- Nowell, G., Kempton, P., Noble, S., Fitton, J., Saunders, A., Mahoney, J., and Taylor, R., 1998, High precision Hf isotope measurements of MORB and OIB by thermal ionisation mass spectrometry: insights into the depleted mantle: *Chemical Geology*, v. 149, no. 3, p. 211–233.
- Ohara, Y., Stern, R.J., Ishii, T., Yurimoto, H., and Yamazaki, T., 2002, Peridotites from the Mariana Trough: first look at the mantle beneath an active back-arc basin: *Contributions to Mineralogy and Petrology*, v. 143, no. 1, p. 1–18, <https://doi.org/10.1007/s00410-001-0329-2>.
- Omidvar, M., Safari, A., Vaziri-Moghaddam, H., and Ghalavand, H., 2018, Foraminiferal biostratigraphy of Upper Cretaceous (Campanian–Maastrichtian) sequences in the Peri-Tethys basin; Moghan area, NW Iran: *Journal of African Earth Sciences*, v. 140, p. 94–113, <https://doi.org/10.1016/j.jafrearsci.2018.01.002>.
- Omrani, H., Moazzen, M., Oberhansli, R., Altenberger, U., and Lange, M., 2013, The Sabzevar blueschists of the North-Central Iranian micro-continent as remnants of the Neotethys-related oceanic crust subduction: *International Journal of Earth Sciences*, v. 102, no. 5, p. 1491–1512, <https://doi.org/10.1007/s00531-013-0881-9>.
- Ozawa, S., Shinjo, R., Lo, C.H., Jahn, B.M., Hoang, N., Sasaki, M., Ishikawa, K., Kano, H., Hoshi, H., Xenophonos, C., and Wakabayashi, J., 2012, Geochemistry and geochronology of the Troodos ophiolite: An SSZ ophiolite generated by subduction initiation and an extended episode of ridge subduction?: *Lithosphere*, v. 4, no. 6, p. 497–510, <https://doi.org/10.1130/L205.1>.
- Pearce, J.A., 2008, Geochemical fingerprinting of oceanic basalts with applications to ophiolite classification and the search for Archean oceanic crust: *Lithos*, v. 100, no. 1–4, p. 14–48, <https://doi.org/10.1016/j.lithos.2007.06.016>.
- Pearce, J.A., and Peate, D.W., 1995, Tectonic Implications of the Composition of Volcanic Arc Magmas: Annual Review of Earth and Planetary Sciences, v. 23, p. 251–285, <https://doi.org/10.1146/annurev.earth.23.050195.001343>.
- Pearce, J.A., and Robinson, P.T., 2010, The Troodos ophiolite complex probably formed in a subduction initiation, slab edge setting: *Gondwana Research*, v. 18, no. 1, p. 60–81, <https://doi.org/10.1016/j.gr.2009.12.003>.
- Pearce, J.A., Harris, N.B.W., and Tindle, A.G., 1984, Trace-element discrimination diagrams for the tectonic interpretation of granitic-rocks: *Journal of Petrology*, v. 25, no. 4, p. 956–983, <https://doi.org/10.1093/ptrology/25.4.956>.
- Pearce, J.A., Kempton, P., Nowell, G., and Noble, S., 1999, Hf-Nd element and isotope perspective on the nature and provenance of mantle and subduction components in Western Pacific arc-basin systems: *Journal of Petrology*, v. 40, no. 11, p. 1579–1611, <https://doi.org/10.1093/ptrology/40.11.1579>.
- Pearce, J.A., Barker, P.F., Edwards, S.J., Parkinson, I.J., and Leat, P.T., 2000a, Geochemistry and tectonic significance of peridotites from the South Sandwich arc-basin system, South Atlantic: *Contributions to Mineralogy and Petrology*, v. 139, no. 1, p. 36–53, <https://doi.org/10.1007/s004100050572>.
- Pearce, J.A., Barker, P.F., Edwards, S.J., Parkinson, I.J., and Leat, P.T., 2000b, Geochemistry and tectonic significance of peridotites from the South Sandwich arc-basin system, South Atlantic: *Contributions to Mineralogy and Petrology*, v. 139, p. 36–53, <https://doi.org/10.1007/s004100050572>.
- Peate, D.W., and Pearce, J.A., 1998, Causes of spatial compositional variations in Mariana arc lavas: Trace element evidence: *The Island Arc*, v. 7, no. 3, p. 479–495, <https://doi.org/10.1111/j.1440-1738.1998.00205.x>.
- Pirnia, T., Arai, S., Tamura, A., Ishimaru, S., and Torabi, G., 2014, Sr enrichment in mantle pyroxenes as a result of plagioclase alteration in Iherzolite: *Lithos*, v. 196, p. 198–212, <https://doi.org/10.1016/j.lithos.2014.03.008>.
- Reagan, M.K., Ishizuka, O., Stern, R.J., Kelley, K.A., Ohara, Y., Blichert-Toft, J., Bloomer, S.H., Cash, J., Fryer, P., Hanan, B.B., Hickey-Vargas, R., Ishii, T., Kimura, J.I., Peate, D.W., Rowe, M.C., and Woods, M., 2010, Fore-arc basalts and subduction initiation in the Izu-Bonin-Mariana system: *Geochemistry Geophysics Geosystems*, v. 11, <https://doi.org/10.1029/2009GC002871>.
- Robinson, P.T., Trumbull, R.B., Schmitt, A., Yang, J.S., Li, J.W., Zhou, M.F., Erzinger, J., Dare, S., and Xiong, F.H., 2015, The origin and significance of crustal minerals in ophiolitic chromitites and peridotites: *Gondwana Research*, v. 27, no. 2, p. 486–506, <https://doi.org/10.1016/j.gr.2014.06.003>.
- Ross, K., and Elthon, D., 1993, Cumulates from strongly depleted mid-ocean-ridge basalt: *Nature*, v. 365, no. 6449, p. 826, <https://doi.org/10.1038/365826a0>.
- Rossetti, F., Nasrabad, M., Vignaroli, G., Theye, T., Gerdes, A., Razavi, M.H., and Vaziri, H.M., 2010, Early Cretaceous migmatitic mafic granulites from the Sabzevar range (NE Iran): implications for the closure of the Mesozoic peri-Tethyan oceans in central Iran: *Terra Nova*, v. 22, no. 1, p. 26–34, <https://doi.org/10.1111/j.1365-3121.2009.00912.x>.
- Rossetti, F., Nasrabad, M., Theye, T., Gerdes, A., Monie, P., Lucci, F., and Vignaroli, G., 2014, Adakite differentiation and emplacement in a subduction channel: The late Paleocene Sabzevar magmatism (NE Iran): *Geological Society of America Bulletin*, v. 126, no. 3–4, p. 317–343, <https://doi.org/10.1130/B30913.1>.
- Saccani, E., Bortolotti, V., Marroni, M., Pandolfi, L., Photiadis, A., and Principi, G., 2008, The Jurassic Association of Backarc Basin Ophiolites and Calc-Alkaline Volcanics in the Guevgueli Complex (Northern Greece): Implication for the Evolution of the Vardar Zone: *Ophiolite*, v. 33, no. 2, p. 209–227.
- Saccani, E., Allahyari, K., Beccaluva, L., and Bianchini, G., 2013, Geochemistry and petrology of the Kerman-shah ophiolites (Iran): Implication for the interaction between passive rifting, oceanic accretion, and OIB-type components in the Southern Neo-Tethys Ocean: *Gondwana Research*, v. 24, no. 1, p. 392–411, <https://doi.org/10.1016/j.gr.2012.10.009>.
- Sandeman, H.A., Hamner, S., Tella, S., Armitage, A.A., Davis, W.J., and Ryan, J.J., 2006, Petrogenesis of Neoproterozoic volcanic rocks of the MacQuoid supracrustal belt: A back-arc setting for the northwestern Hearne subdomain, western Churchill Province, Canada: *Precambrian Research*, v. 144, no. 1–2, p. 140–165, <https://doi.org/10.1016/j.precamres.2005.11.001>.
- Sanfilippo, A., Dick, H.J.B., and Ohara, Y., 2013, Melt-rock reaction in the mantle: Mantle troctolites from the Parece Vela ancient back-arc spreading center: *Journal of Petrology*, v. 54, no. 5, p. 861–885, <https://doi.org/10.1093/ptrology/egs089>.
- Sarifikioğlu, E., Ozen, H., and Winchester, J.A., 2009, Petrogenesis of the Refahiye Ophiolite and its tectonic significance for Neotethyan ophiolites along the Izmir-Ankara-Erzincan Suture Zone: *Turkish Journal of Earth Sciences*, v. 18, no. 2, p. 187–207.
- Shafaii Moghadam, H., Zaki Khedr, M., Arai, S., Stern, R.J., Ghorbani, G., Tamura, A., and Ottley, C.J., 2015b, Arc-related harzburgite–dunite–chromitite complexes in the mantle section of the Sabzevar ophiolite, Iran: A model for formation of podiform chromitites: *Gondwana Research*, v. 27, no. 2, p. 575–593, <https://doi.org/10.1016/j.gr.2013.09.007>.
- Shaw, S.E., and Flood, R.H., 2009, Zircon Hf isotopic evidence for mixing of crustal and silicic mantle-derived magmas in a zoned granite pluton, eastern Australia: *Journal of Petrology*, v. 50, no. 1, p. 147–168, <https://doi.org/10.1093/ptrology/egn078>.
- Shervais, J.W., 1982, Ti-V plots and the petrogenesis of modern and ophiolite lavas: *Earth and Planetary Science Letters*, v. 59, no. 1, p. 101–118, [https://doi.org/10.1016/0012-821X\(82\)90120-0](https://doi.org/10.1016/0012-821X(82)90120-0).
- Shinjo, R., 1999, Geochemistry of high Mg andesites and the tectonic evolution of the Okinawa Trough Ryukyu arc system: *Chemical Geology*, v. 157, no. 1–2, p. 69–88, [https://doi.org/10.1016/S0009-2541\(98\)00199-5](https://doi.org/10.1016/S0009-2541(98)00199-5).
- Shinjo, R., Chung, S.L., Kato, Y., and Kimura, M., 1999, Geochemical and Sr-Nd isotopic characteristics of volcanic rocks from the Okinawa Trough and Ryukyu Arc: Implications for the evolution of a young, intracontinental back arc basin: *Journal of Geophysical Research. Solid Earth*, v. 104, no. B5, p. 10591–10608, <https://doi.org/10.1029/1999JB900040>.
- Shojaat, B., Hassani, A.A., Mobasher, K., and Ghazi, A.M., 2003, Petrology, geochemistry and tectonics of the Sabzevar ophiolite, North Central Iran: *Journal of Asian Earth Sciences*, v. 21, no. 9, p. 1053–1067, [https://doi.org/10.1016/S1367-9120\(02\)00143-8](https://doi.org/10.1016/S1367-9120(02)00143-8).
- Sorbadere, F., Schiano, P., Metrich, N., and Bertagnini, A., 2013, Small-scale coexistence of island-arc- and enriched-MORB-type basalts in the central Vanuatu arc: Contributions to Mineralogy and Petrology, v. 166, no. 5, p. 1305–1321, <https://doi.org/10.1007/s00410-013-0928-8>.
- Stern, R.J., 2002, Subduction zones: *Reviews of Geophysics*, v. 40, no. 4, <https://doi.org/10.1029/2001RG000108>.
- Stern, R.J., 2004, Subduction initiation: spontaneous and induced: *Earth and Planetary Science Letters*, v. 226, no. 3–4, p. 275–292, [https://doi.org/10.1016/S0012-821X\(04\)00498-4](https://doi.org/10.1016/S0012-821X(04)00498-4).
- Stern, R.J., and Dickinson, W.R., 2010, The Gulf of Mexico is a Jurassic backarc basin: *Geosphere*, v. 6, no. 6, p. 739–754, <https://doi.org/10.1130/GES00585.1>.
- Stern, R.J., and Gerya, T., 2017, Subduction initiation in nature and models: A review: *Tectonophysics*, v. 746, p. 173–198, <https://doi.org/10.1016/j.tecto.2017.10.014>.
- Stracke, A., Hofmann, A.W., and Hart, S.R., 2005, FOZO, HIMU, and the rest of the mantle zoo: *Geochemistry Geophysics Geosystems*, v. 6, <https://doi.org/10.1029/2004GC000824>.
- Tadayon, M., Rossetti, F., Zattin, M., Nozaem, R., Calzolari, G., Madanipour, S., and Salvini, F., 2017, The post-Eocene evolution of the Doruneh fault region (central Iran): The intraplate response to the reorganization of the Arabia-Eurasia collision zone: *Tectonics*, v. 36, p. 3038–3064, <https://doi.org/10.1002/2017TC004595>.
- Tadayon, M., Rossetti, F., Zattin, M., Calzolari, G., Nozaem, R., Salvini, F., Faccenna, C., and Khodabakhshi, P., 2018, The long-term evolution of the Doruneh fault region (central Iran): A key to understanding the spatio-temporal tectonic evolution in the hinterland of the Zagros convergence zone: *Geological Journal*, v. 54, p. 1454–1479, <https://doi.org/10.1002/gj.3241>.
- Taylor, B., and Martinez, F., 2003, Back-arc basin basalt systematics: *Earth and Planetary Science Letters*, v. 210, no. 3–4, p. 481–497, [https://doi.org/10.1016/S0012-821X\(03\)00167-5](https://doi.org/10.1016/S0012-821X(03)00167-5).
- Thomas, J.-C., Grasso, J.-R., Bossu, R., Martinod, J., and Nurtaev, B., 1999, Recent deformation in the Turan and South Kazakh platforms, western central Asia, and its relation to Arabia-Asia and India-Asia collisions: *Tectonics*, v. 18, no. 2, p. 201–214, <https://doi.org/10.1029/1998TC900027>.
- Tian, L.Y., Castillo, P.R., Hilton, D.R., Hawkins, J.W., Hanan, B.B., and Pietruszka, A.J., 2011, Major and trace element and Sr-Nd isotope signatures of the northern Lau Basin lavas: Implications for the composition and dynamics of the back-arc basin mantle: *Journal of Geophysical Research. Solid Earth*, v. 116, <https://doi.org/10.1029/2011jb008791>.
- Tiepolo, M., Oberti, R., Zanetti, A., Vannucci, R., and Foley, S.F., 2007, Trace-element partitioning between amphibole and silicate melt: Reviews in Mineralogy and Geochemistry, v. 67, no. 1, p. 417–452, <https://doi.org/10.2138/rmg.2007.67.11>.
- Todd, E., Gill, J.B., Wysoczanski, R.J., Hergt, J., Wright, I.C., Leybourne, M.I., and Mortimer, N., 2011, Hf isotopic evidence for small-scale heterogeneity in the mode of mantle wedge enrichment: Southern Havre Trough and South Fiji Basin back arcs: *Geochemistry Geophysics Geosystems*, v. 12, <https://doi.org/10.1029/2011GC003683>.
- Üner, T., Cakir, U., Ozdemir, Y., and Arat, I., 2014, Geochemistry and origin of plagiogranites from the Eldivan Ophiolite, Cankiri (Central Anatolia, Turkey): *Geologica Carpathica*, v. 65, no. 3, p. 195–205, <https://doi.org/10.2478/geoca-2014-0013>.
- Vaezi Pour, M. J., Alavi Tehrani, N., Behrouzi, A., and Kholghi, M. H., 1992, Geological Map of the Torbat-e-Heydarieh: *Geological Survey of Iran*.
- van Hinsbergen, D.J.J., Peters, K., Maffione, M., Spakman, W., Guillmette, C., Thieulot, C., Plumper, O., Gurer, D., Brouwer, F.M., Aldanmaz, E., and Kaymakci,

- N., 2015, Dynamics of intraoceanic subduction initiation: 2. Suprasubduction zone ophiolite formation and metamorphic sole exhumation in context of absolute plate motions: *Geochemistry Geophysics Geosystems*, v. 16, no. 6, p. 1771–1785, <https://doi.org/10.1002/2015GC005745>.
- Verdel, C., Wernicke, B.P., Ramezani, J., Hassanzadeh, J., Renne, P.R., and Spell, T.L., 2007, Geology and thermochronology of Tertiary Cordilleran-style metamorphic core complexes in the Saghand region of central Iran: *Geological Society of America Bulletin*, v. 119, no. 7-8, p. 961–977, <https://doi.org/10.1130/B26102.1>.
- Verdel, C., Wernicke, B.P., Hassanzadeh, J., and Guest, B., 2011, A Paleogene extensional arc flare-up in Iran: *Tectonics*, v. 30, <https://doi.org/10.1029/2010TC002809>.
- Vervoort, J.D., and Blichert-Toft, J., 1999a, Evolution of the depleted mantle: Hf isotope evidence from juvenile rocks through time: *Geochimica et Cosmochimica Acta*, v. 63, no. 3, p. 533–556, [https://doi.org/10.1016/S0016-7037\(98\)00274-9](https://doi.org/10.1016/S0016-7037(98)00274-9).
- Vervoort, J.D., Patchett, P.J., Blichert-Toft, J., and Albarede, F., 1999, Relationships between Lu-Hf and Sm-Nd isotopic systems in the global sedimentary system: *Earth and Planetary Science Letters*, v. 168, no. 1-2, p. 79–99, [https://doi.org/10.1016/S0012-821X\(99\)00047-3](https://doi.org/10.1016/S0012-821X(99)00047-3).
- Whattam, S.A., and Stern, R.J., 2011, The ‘subduction initiation rule’: a key for linking ophiolites, intra-oceanic forearcs, and subduction initiation: *Contributions to Mineralogy and Petrology*, v. 162, no. 5, p. 1031–1045, <https://doi.org/10.1007/s00410-011-0638-z>.
- Woodhead, J., Stern, R.J., Pearce, J., Hergt, J., and Vervoort, J., 2012, Hf-Nd isotope variation in Mariana Trough basalts: The importance of “ambient mantle” in the interpretation of subduction zone magmas: *Geology*, v. 40, no. 6, p. 539–542, <https://doi.org/10.1130/G32963.1>.
- Woodhead, J.D., and Devey, C.W., 1993, *Geochemistry of the Pitcairn Seamounts 1: Character and Temporal Trends: Source Earth and Planetary Science Letters*, v. 116, no. 1-4, p. 81–99.
- Woodhead, J.D., Hergt, J., Davidson, J., and Eggins, S., 2001, Hafnium isotope evidence for ‘conservative’ element mobility during subduction zone processes: *Earth and Planetary Science Letters*, v. 192, no. 3, p. 331–346, [https://doi.org/10.1016/S0012-821X\(01\)00453-8](https://doi.org/10.1016/S0012-821X(01)00453-8).
- Yogodzinski, G.M., Vervoort, J.D., Brown, S.T., and Gersen, M., 2010, Subduction controls of Hf and Nd isotopes in lavas of the Aleutian island arc: *Earth and Planetary Science Letters*, v. 300, no. 3-4, p. 226–238, <https://doi.org/10.1016/j.epsl.2010.09.035>.
- Zarrinkoub, M.H., Pang, K.N., Chung, S.L., Khatib, M.M., Mohammadi, S.S., Chiu, H.Y., and Lee, H.Y., 2012, Zircon U-Pb age and geochemical constraints on the origin of the Birjand ophiolite, Sistan suture zone, eastern Iran: *Lithos*, v. 154, p. 392–405, <https://doi.org/10.1016/j.lithos.2012.08.007>.

SCIENCE EDITOR: BRADLEY S. SINGER
ASSOCIATE EDITOR: MASSIMO MATTEI

MANUSCRIPT RECEIVED 15 JUNE 2018
REVISED MANUSCRIPT RECEIVED 13 MAY 2019
MANUSCRIPT ACCEPTED 19 JUNE 2019

Printed in the USA